Hydrocarbon Oxidation in the Exhaust Port and Runner of a Spark Ignition Engine

by

Kristine Drobot

Bachelor of Science in Mechanical Engineering
University of Michigan, Ann Arbor
(1991)

Submitted to the
Department of Mechanical Engineering
in Partial Fulfillment of the Requirements for the
Degree of

MASTER OF SCIENCE
in Mechanical Engineering
at the

MASSACHUSETTS INSTITUTE OF TECHNOLOGY

February 1994

Signature of Author_____
Department of Mechanical Engineering
January 28, 1994

Certified by_____
Wai K.Cheng
Professor, Mechanical Engineering Department
Thesis Supervisor

Accepted by_____
Ain A. Sonin
Chairman, Department Graduate Program

(This page has been intentionally left blank.)

Hydrocarbon Oxidation in the Exhaust Port and Runner of a Spark Ignition Engine

by Kristine Drobot

Submitted to the Department of Mechanical Engineering in partial fulfillment of the requirements for the Degree of Master of Science in Mechanical Engineering

ABSTRACT

An exhaust gas quenching experiment was conducted to study the evolution of HC emissions and the extent of HC oxidation in the exhaust port and runner of a spark ignition engine. Fuel composition and engine parameter effects were of particular interest. The fuel set consisted of gasoline, several alkanes (methane, ethane, propane, n-butane, iso-octane), an alkene (ethene) and an aromatic (toluene); all fuel composition experiments were completed at a light load condition. The engine parameter set included engine speed, load, spark timing, equivalence ratio and coolant temperature; experiments involved mostly single parameter variations about a light load condition.

The cylinder-exit HC emissions varied significantly over the set of fuels tested. There was no significant fuel dependency in the percentage of HC oxidation in the exhaust port/runner system, which ranged from 35 to 45%. A substantial portion of the oxidation occurred in the exhaust port. Speciated HC emissions identified unburned fuel as the major cylinder-exit species. The unburned fuel contribution ranged from 80 to 95% for methane, ethene and toluene and from 40 to 70% for the non-methane alkane fuels. Changes in the species distributions for the non-methane alkane fuels were observed in both the port and runner. Alkenes, the most reactive species in the formation of photochemical smog, were the dominant non-fuel species. Hence, the benefit of HC oxidation was accompanied by an increase in photochemical reactivity.

Independent increases in engine speed and load produced decreases in the percentage of HC oxidation in the exhaust port/runner system. Higher temperatures due to spark retard increased HC oxidation from approximately 38% at MBT to approximately 53% at 12 degrees retard. Fuel lean conditions yielded higher oxidation levels (42%) than did fuel rich conditions (27%) due to the O_2 availability. There was negligible change in oxidation level over the coolant temperature range tested.

Thesis Advisor: Wai K. Cheng
Associate Professor, Department of Mechanical Engineering

(This page has been intentionally left blank.)

ACKNOWLEDGMENTS

This experiment was funded exclusively by and conducted entirely at the Ford Motor Company. However, much appreciation is extended to the Engine/Fuels Interactions Consortium for their input. Member companies include the Chevron Research Corporation, Department of Energy, Exxon Research and Engineering Company, Nippon Oil Company, Ltd. and Shell Oil Company.

It has been said that this is the easiest part of the thesis to write. For me, it is the hardest. How can I share the joy and tears, victories and failures, challenge and perseverance that filled each of my days for the past two years? I cannot. But I can share about the people that made these past two years possible:

Professors Wai Cheng and John Heywood, I extend my sincerest thanks for your guidance and technical expertise. And Professor Cheng, I am forever grateful for your concern, understanding and encouragement.

Rod Tabaczynski, George Davis, Fred Trinker and William Kaiser, your interest and enthusiasm towards my research have inspired me often during the difficult times.

Dave Cotton, it was a pleasure working with you and your flexibility will not be forgotten. I no longer consider you my technician but rather my friend.

Jim Ryan, you have been a light in my darkness, an attentive ear and a friend. There is nothing more I could ask for.

Andrea Kazal, you always understood me and my schedule. Thanks for walking with me and helping me grow.

Lisa Chou and Jude Federspiel, your late-night visits and talks kept me strong through the good and bad times.

Charlotte Huang, you made coming home and hanging out something to look forward to.

Dan Zachary, despite trying to finish your own thesis you saw fit to keep my spirits up. I am grateful for your joy.

Dad, Mom, Stephanie and Roberta, though we were 800 miles away for the past two years, I always knew that you loved me and supported me. I love you, too.

Father, you have given me hope, a future and a purpose--just like you promised. I am eternally grateful for our relationship.

Kristine Drobot

"It is finished." --John 19:30

(This page has been intentionally left blank.)

TABLE OF CONTENTS

LIST OF TABLES

LIST OF FIGURES

Chapter 1

Introduction

1.1 Motivation

Increasing concern for the environment has lead to stricter government regulation [1] of hydrocarbon (HC) emissions from passenger vehicles. The 1995 California Ultra Low Emissions Vehicle (ULEV) standard of 0.04 gm/mile is already ten times lower than the 1980 HC emissions standard of 0.39 gm/mile. In the past regulations and standards have been based solely on the total non-methane organic gas (NMOG) coming from the vehicle as determined by the Federal Testing Procedure. Speciated HC emissions are of increasing importance because the State of California will soon regulate HC emissions based on their reactivity in forming photochemical smog in the atmosphere [2].

The challenge of lowering HC emissions has fueled significant research efforts, especially in understanding the sources of unburned HC. A recent study indicated that the main HC formation mechanisms in a warmed-up engine were crevices, oil layer absorption/desorption, deposit layer adsorption/desorption and liquid fuel effects; their

estimated contributions to the total engine-out HC emissions were 38%, 16%, 16% and 20%, respectively [3]. As a result of these mechanisms, roughly 8.3% of the fuel that entered the cylinder would escape primary combustion [3]. Should the unburned HC enter the bulk gas early enough, they would be oxidized in-cylinder during expansion and exhaust. Still a large fraction of what leaves the cylinder is unburned HC [4].

With a HC conversion efficiency of approximately 90%, the modern catalyst is critical in the HC removal process. However, during engine warm-up when the HC emissions are especially high [5], the catalyst is still cold and ineffective. At this time the exhaust port and runner oxidation processes become the major HC removal process outside the cylinder. Therefore, tracking the total HC emissions as well as quantifying the extent of the HC oxidation in the exhaust port/runner are of considerable interest.

1.2 Background

Back in 1981 Mendillo and Heywood [6] determined the fraction of unburned HC reduced in the exhaust port of a spark ignition engine. They accomplished this by injecting quench gas (CO_2) into the exhaust system to lower the exhaust gas temperature and freeze or quench the HC oxidation reactions. Quench gas was introduced into the exhaust port through either a hollowed out sodium valve stem or an adjustable probe that traversed the exhaust port. The experiment was completed on a gasoline-fueled CFR engine over a range of different operating conditions. Mendillo found that oxidation was dominated by variations in exhaust gas temperature, port residence time and O_2 concentration. Oxidation levels ranges from 2-37% in the exhaust port over the range of operating conditions tested.

This present is similar to that of reference [6], but with important differences: (i) the engine used had a modern exhaust port geometry which is typical of current

production, and (ii) exhaust speciation was carried out. Thus this study updates, complements and expands on the data of reference [6].

1.3 Objective

At present the knowledge of HC oxidation in the exhaust port and runner of a spark ignition engine is incomplete. This experiment aimed at contributing the following:

1. Investigating the effects of engine parameters and fuel composition on HC oxidation;

2. Quantifying the extent of HC oxidation in the exhaust port and runner; and

3. Studying the evolution of total HC emissions and individual HC species through the exhaust system.

1.4 Approach

Like Mendillo, a quenching experiment was conducted, whereby quench gas was injected into the exhaust system to freeze the HC oxidation reactions. Once the HC emissions were corrected for dilution due to the injection of quench gas, the pre-oxidation HC emissions were compared to the post-oxidation HC measured under normal (i.e. no quenching) exhaust conditions. Speciated HC emissions were also measured.

Chapter 2

Experimental Apparatus

2.1 Engine and Data Acquisition

The engine used in this experiment was a single-cylinder, 4-stroke engine which comprised a developmental two-valve, Ford Escort head atop a Waukeshau base. The intake and exhaust port geometries were representative of modern two-valve engine designs. A summary of the engine specifications is listed in Table 2.2-1. The engine was coupled to a DC motor dynamometer with a 50 hp absorbing rating.

Both the spark timing and fuel injection were controlled by an electronic control unit, known as the EFI-III, which received a reference pulse every TDC compression. Liquid fuels were injected directly into the intake port, while the gaseous fuels were introduced in the intake manifold approximately 1.8 meters from the valve.

Air delivery to the intake system employed a critical air orifice system. Its flow was calculated by the data acquisition system from the given pre-orifice pressure, orifice size and air temperature.

An NTK air/fuel (A/F) meter used both an exhaust gas oxygen (EGO) sensor and the fuel's hydrogen-to-carbon ratio to determine the intake A/F ratio.

The engine was water cooled. Although coolant flow to the head and block was supplied from the same line, coolant flow within the head and block was separate.

Type K thermocouples measured all intake, exhaust, coolant and air temperatures. The exhaust gas temperature, in particular, was a time-averaged measurement made at the port exit approximately 7 centimeters from the valve seat using a shielded thermocouple. Cylinder and port pressures were monitored using Kistler 6123A and 4045 pressure transducers, respectively.

A manometer measured the exhaust back pressure, which could be adjusted manually. Adjustment was necessary to maintain normal back pressure of ½ inch Hg over atmospheric during the injection of quench gas into the exhaust system. Otherwise, the exhaust gas flow dynamics would have been severely disrupted.

All operating condition and emissions data were collected using a Masscomp data acquisition system. Each data point was averaged over a sample of 100 cycles.

2.2 Quench Gas Injection System

The quench gas injection system was designed to introduce a timed and directed jet of quench gas into the exhaust system. Rapid cooling of the exhaust gas HC oxidation reactions resulted.

2.2.1 Quench Gas Selection

The ideal quench gas was one that had a high heat capacity and was stable under the thermal and chemical environments associated with exhaust. Relative to a low heat capacity quench gas, a high heat capacity gas would reduce the mass flow needed for

adequate quenching. This would help avoid excessive cooling of the exhaust valve and substantial changes in exhaust back pressure. Availability and low cost, in addition to satisfying the previous requirements, made carbon dioxide (CO_2) the ideal quench gas. Commercial grade (99.8% pure), bone dry CO_2 was sufficient for this experiment.

2.2.2 Quench Gas Injection Control

The quench gas injection system illustrated in Figure 2.2-1 was designed to pulse jets of quench gas in phase with the exhaust valve open period when cooling was needed most. Controlled injection helped to minimize quench gas backflow during overlap which could affect in-cylinder processes such as HC oxidation.

The injection control process, indicated in Figure 2.2-1, was as follows: a magnetic proximity pick-up (a) generated a TTL pulse once every 720°CA for the EFI-III. The EFI-III recognized the pulse as TDC compression and sent this information (b) to a computer. At the computer a value referred to as a preset was input and sent to the EFI-III (c). This preset was the crank angle (relative to TDC compression) when the 2-way, normally closed solenoid valve should be triggered to open. A summary of the solenoid valve specifications is listed in Table 2.2-1. Selection of the preset, which was based on the solenoid valve response time, exhaust valve timing and engine speed, is covered in detail in Section 3.1. The EFI-III then triggered (d) the pulse generator. When triggered, the pulse generator sent (e) the manually-inputted pulse width to both the oscilloscope for viewing and the controller for triggering. The pulse width indicated how long the solenoid valve was to remain open. The controller amplified the pulse width to a 24 volt DC signal and sent it (f) to the solenoid valve. Following the response time delay, the solenoid valve opened and remained open for the duration of the set pulse width. While the solenoid valve was open, quench gas continued to flow from the supply bottle (g) at the predetermined, regulated delivery pressure to fill the supply line. To warm the quench gas and prevent the solenoid valve from freezing up, the supply line was wrapped with heat

tape (h) maintained at 200°F. When the quench gas flowed through the open solenoid valve and past the pressure transducer (Micro Switch #242PC250G) (i), the transducer returned its signal (j) to the controller. The latter enabled the pressure transducer signal to be viewed on an oscilloscope (k) such that the quench gas delivery pressure could be set. Once past the pressure transducer, the quench gas entered into one of two injectors (l).

The quench gas injectors were responsible for directing the flow of quench gas into the exhaust system. The injector arrangement is illustrated in Figure 2.2-2. Pictured from left to right are: (1) an injector that placed quench gas directly behind the exhaust valve; (2) an injector that directed jets of quench gas at the port exit; (3) a flange that housed a thermocouple radiation shield; and (4) a flange mated to an exhaust manifold equipped with a thermocouple. The exhaust gas flowed through the port cross-section-shaped passages in the direction indicated. Injector (1) was the combination of one stainless steel 304 (SS304) flange and seven welded and drawn SS304 tubes (0.043" OD and 0.0375" ID). The injector, shown again in Figure 2.2-3, was bolted up against the head such that the tubes extended into and laid along the bottom of the exhaust port. During injection, pressurized quench gas would flow into the channel and out the tubes as jets. The location of the jets put quench gas directly behind the exhaust valve, establishing a quench plane at the cylinder exit. A quench plane was where the quench gas interacted with the exhaust gas to freeze the oxidation reactions. Though the tubes laid along the bottom of the port, their orientation did not permit quench gas flow directly into the combustion chamber. The wrap-around configuration of the tubes and the location of the jets promoted penetration of the quench gas jets into the cross-flowing exhaust gas. This insured adequate mixing and rapid cooling of the exhaust gas. Injector (2) was a SS304 flange with seven, vertically-oriented holes. It was placed directly behind and up against injector (1) as shown in Figure 2.2-3. During injection, pressurized quench gas would fill the channel and flow out the tubes to establish a quench plane at the port exit. Because both injectors were imbedded in the flanges, the head required no structural modification

but merely simple additions to existing hardware. As a result of this approach, installation and removal were simplified.

2.3 Emissions Analyzers

Both the overall and speciated HC emissions were measured in this experiment. In addition, the normal exhaust gas were used to quantify the extent of HC oxidation and to quantify the mass flow rate of quench gas from which a dilution correction factor was derived. Details related to the use of emissions measurements for these purposes are covered in Section 3.4. All samples were drawn from a large exhaust gas mixing tank at the runner exit by a heated sample line. Measurements were recorded once steady-state levels were reached and represent bulk, pre-catalyst emissions concentrations.

The normal exhaust measurements were obtained from the HORIBA emissions bench which housed devices that measured the following exhaust gas emissions: carbon monoxide (CO), carbon dioxide (CO_2), oxygen (O_2), oxides of nitrogen (NO_x) and hydrocarbons (HC). The CO_2, NO_x and HC emissions were of particular interest. The CO_2 emissions were measured by a non-dispersive infra-red detector (NDIR). The NO_x were measured by chemi-luminescence. A heated flame ionization detector (HFID) measured the total HC emissions. Emissions bench measurement error was estimated at ±1% under normal exhaust conditions and ±2% once corrected for dilution due to quench gas injection.

A gas chromatograph (GC) speciated the HC compounds (up to C_8) found in the exhaust gas. GC measurement error was estimated at ±5% for all measurements and an absolute detectability error of ±0.1% for minor species that contributed less than 1% of the total HCs.

TABLE 2.1-1 Summary of Engine Specifications

Model	Ford Escort head atop a Waukeshau base
Type	Single-cylinder, 4-stroke engine; 2-valve developmental head with directed intake flow for swirl
Bore	82.0 mm
Stroke	88.0 mm
Displacement	464.7 cc
Compression Ratio	9:1
Valve Timing	
Exhaust Valve Open	59° BBDC
Exhaust Valve Close	17° ATDC
Intake Valve Open	15° BTDC
Intake Valve Close	61° ABDC

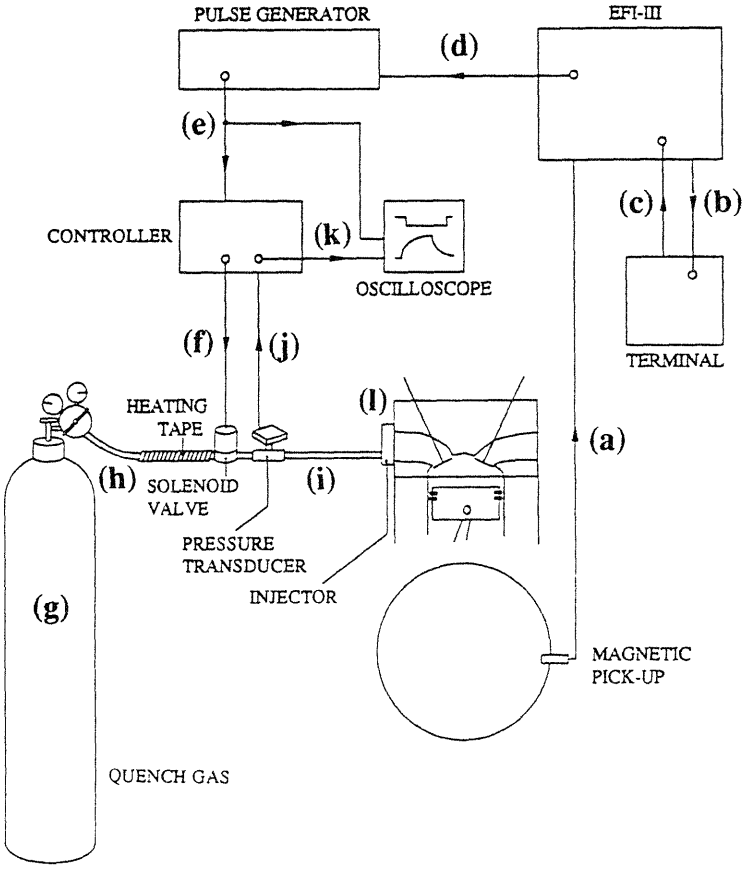

FIGURE 2.2-1 Quench gas injection system.

TABLE 2.2-1 Summary of Solenoid Valve Specifications

Manufacturer	KIP Incorporated
Part Number	UL241114-0110-24VDC
Valve Type	2-way normally closed
Port Type	1/8" NPTF
Orifice Diameter	3/32 "
Cv Factor	0.175
Maximum Operating Pressure Differential	250 psi
Response Time	10 msec

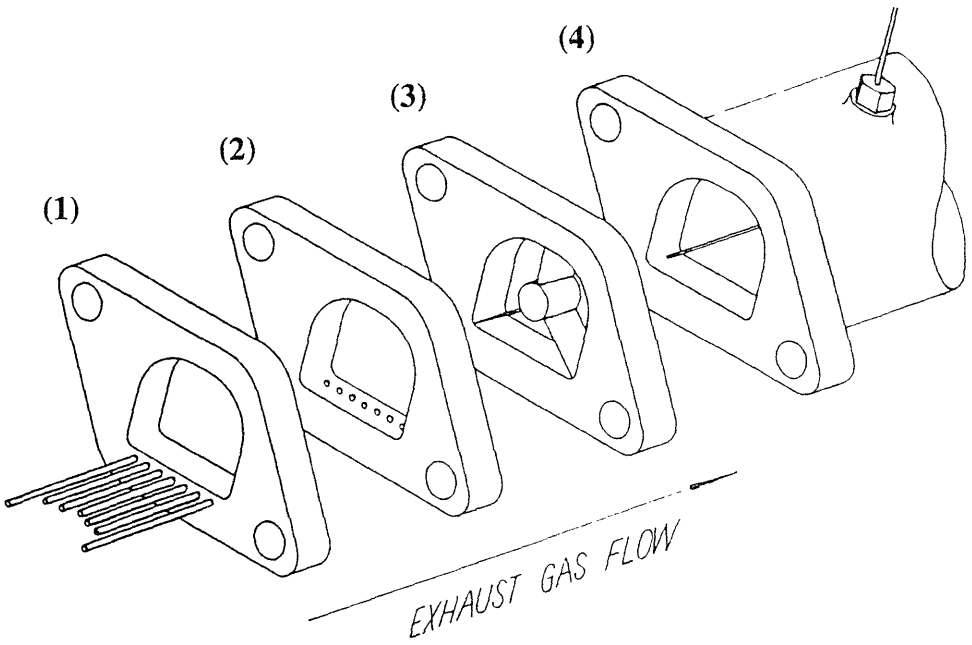

FIGURE 2.2-2 Quench gas injectors pictured with existing exhaust hardware; (1) establishes the cylinder exit quench plane; (2) establishes the port exit quench plane; (3) supports the thermocouple radiation shield; (4) houses the thermocouple.

(a)

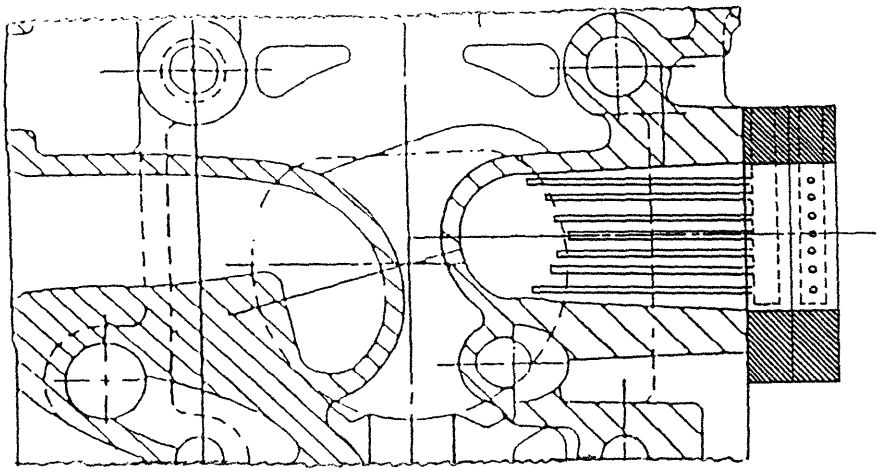

(b)

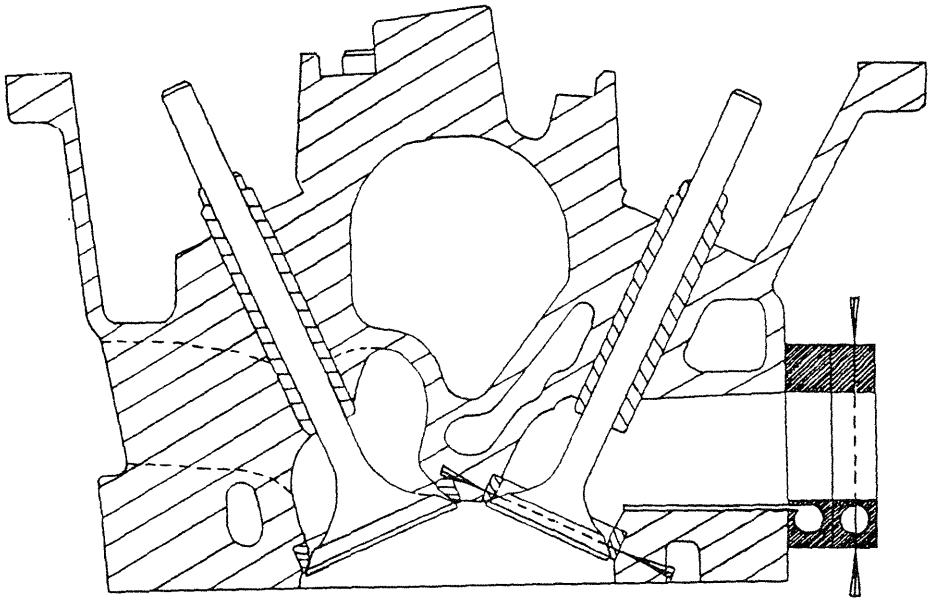

FIGURE 2.2-3 Orientation of the quench gas injectors (a) relative to the head and (b) within the exhaust port.

Chapter 3

Experimental Procedure

3.1 Test Matrices

Two experimental matrices were developed to investigate fuel composition and engine parameter effects on the evolution of HC emissions and the extent of HC oxidation. Both matrices were centered about the baseline engine operating condition listed in Table 3.1-1. This operating condition is representative of the street cruise condition in the 23-cycle Federal Testing Procedure for vehicle emissions except for the fuel equivalence ratio Φ. The value of Φ is set at 0.9 because the HC emissions level is not sensitive to Φ at this value.

3.1.1 Fuel Composition Matrix

The set of fuels listed in Table 3.1-2 were tested to study the fuel composition effect on HC emissions and oxidation. Included in the set were a number of alkanes (methane, ethane, propane, n-butane, iso-octane), an alkene (ethene), an aromatic (toluene) and a full

blend gasoline. Within this set was the potential to compare gaseous to liquid, unsaturated to saturated and low to high molecular weight fuels. Appendix A indicates the fuels with total and speciated HC emissions available at the cylinder and port exits.

3.1.2 Engine Parameter Matrix

Hydrocarbon oxidation is controlled by the exhaust gas temperature, O_2 concentration, mass flow rate and port residence time [7]. The engine parameters that govern these exhaust conditions were used to define the engine parameter matrix. The parameters included: engine speed, engine load, spark timing, equivalence ratio and coolant temperature. Each parameter was swept individually about the baseline condition at the levels indicated in Table 3.1-3. A limited set of data was taken where multiple parameters were varied simultaneously.

A complete matrix was run for gasoline, though its baseline equivalence ratio was stoichiometric (Φ=1.0) rather than lean (Φ=0.9). Stoichiometric operation, which is a more realistic operating condition, was required for validation of a port HC oxidation model. This matrix was only partially completed for propane and iso-octane. A listing of the fuels with total HC emissions data available for each complete or partial single parameter sweep appears in Appendix A.

3.2 Quench Gas Injection Parameters

As implied in Section 2.2.2, many signals were needed to generate a properly timed injection. Among these signals were the pulse width, preset and delivery pressure, which controlled the length of injection, the start of injection and the injection pressure, respectively. Selection and optimization of these quench gas injection parameters was

critical as it directly affected whether quenching was adequate and quench gas back flow during overlap was minimized.

3.2.1 Optimization of Injection Parameters

Quench gas injection was needed for the duration of the exhaust process only. Ideally, the normally-closed solenoid valve, which governed whether or not there was quench gas flow, would open for the 256 crank angle degrees (°CA) exhaust valve open period. There was, however, a substantial valve-overlap period (32 °CA, see also Figure 3.2-1(a)) during which the flow in the exhaust system was in the reverse direction. Because injection during overlap would draw and trap unwanted quench gas into the cylinder and disrupt the next combustion process, the length of injection (set by the pulse width but governed by the solenoid valve) was reduced to 224 °CA. Inputting this to the pulse generator required converting from °CA to milliseconds (msec). At the baseline engine speed of 1500 rpm, 25 msec was the optimal length of injection.

The signal shown in Figure 3.2-1(b) indicates both the length and start of injection for the baseline operating condition. The signal that triggered the solenoid valve to open was not set to trigger at EVO for a number of reasons. First, a 10 msec response delay from the solenoid valve automatically advanced the signal so that quench gas would begin flowing at EVO. Even when the solenoid valve opened, it took time for the quench gas to reach its maximum flow rate, as the pressure trace in Figure 3.2-1(c) indicates. Furthermore, time was required for the injection system downstream of the solenoid valve to purge itself of quench gas even though the volume downstream was minimized. This was critical in minimizing the back flow of quench gas during overlap. Lastly, a cloud of quench gas behind the exhaust valve before EVO would yield more effective quenching, especially during blowdown. The effect of the start of quench gas injection (relative to EVO) on the exhaust gas temperature and the normalized cylinder exit emissions were considered when determining how advanced the start of injection should be given the

optimized length of injection. Results can be found in Figures 3.2-2(a)-(c). While the time-averaged exhaust gas temperature measured during injection did not vary significantly over the range tested, it did indicate increasing temperatures at the extremes. This meant that the start of injection could not be too advanced or too close to EVO otherwise the tail end of the exhaust or blowdown would escape adequate quenching. When normalized by the runner exit emissions, the cylinder exit emissions generated the trends found in Figure 3.2-2(b) and (c). For the NO_x, the ideal timing was the normalization ratio closest to unity; where the NO_x values during injection were highest meant that the in-cylinder temperatures were high indicating that the back flow of quench gas into the cylinder was minimized. In this case both extremes were acceptable. The HC results, on the other hand, indicated that the advanced start of injection timings quenched most adequately; this was concluded from the increase in the normalization ratio as the timing was advanced. Near EVO the ratio and quenching adequacy, in turn, deteriorated dramatically. Altogether the results indicated that advanced start of injection timing quenched more effectively, but that it can not so advanced that the tail end of the exhaust process escapes quenching. At the baseline condition, the ideal timing was determined to be 211 °CA before EVO.

The optimization of the length and start of injection did not in themselves guarantee that sufficient quench gas mass flow rates would be delivered. Optimal delivery pressure was obtained when the cylinder exit HC emissions leveled off. Accompanied by increases in exhaust mass flow rates, load increases required higher delivery pressures to effectively cool the exhaust gas.

3.2.2 Injection Integrity Checks

Having optimized the injection parameters, the quench gas flow rate was checked for sufficient quenching at the cylinder exit plane. As shown in Figure 3.2-3, the cylinder exit HC emissions were measured as a function of quench gas flow rate at both 1500 and 2500

rpm. As the rate of quench gas flow increased from zero, the corrected HC emissions also increased because the quenching effectiveness increased. Eventually, all HC oxidation was quenched and the HC emissions plateaued. Both rates were in the plateau region but not excessively so in order to limit the effects of quench gas backflow. The optimum rates at 1500 and 2500 rpm were 1.25 and 1.44 times the engine mass flow rate, respectively.

To determine the effect of excess CO_2 in-cylinder due to injection, CO_2 was added in increasing amounts to the intake charge only. The air flow, fuel flow and spark timing were fixed at the baseline condition. Up to 4% of the intake charge mass was added CO_2. The effect on IMEP was negligible. The NO_x emissions, shown in Figure 3.2-4, dropped dramatically with the increasing presence of CO_2 because of the sensitivity of NO_x formation to the burned gas temperature. The HC emissions remain virtually unchanged. During quench gas injection at the baseline engine condition, the corrected NO_x decreased to 0.58 of the NO_x under normal exhaust conditions. According to Figure 3.2-4, approximately 0.57% of the inlet charge mass was quench gas that was drawn back into the cylinder. This additional amount of CO_2 had little effect on the HC emissions indicating that the backflow of quench gas into the cylinder would not effect the cylinder exit HC measurements.

3.3 Operating Procedure

The standard operating procedure used throughout the experiment is outlined here and in Figure 3.3-1. It is assumed that the emissions bench has been calibrated. Having selected a fuel and a set of engine conditions, the engine was warmed-up and left running at the desired engine speed. Having measured the friction, the brake mean effective pressure (BMEP) was set such that the single-cylinder's indicated mean effective pressure (IMEP) matched that of a multi-cylinder. While the engine stabilized, the quench gas injection

system was prepared. The quench gas supply line was attached to the appropriate injector (either (1) or (2) according to Figure 2.2-2); the heating tape was turned on and set to 200 °F; and the quench gas injection parameters (length of injection, start of injection and delivery pressure) for the given engine operating condition were inputted manually. The injection system was run briefly to monitor and fine-tune the injection parameter settings. The engine was allowed to reach steady-state at the desired engine speed, load, equivalence ratio and coolant temperature. MBT spark timing was set automatically. If retarded data was desired, then only the spark timing was adjusted at this time; accompanying changes in equivalence ratio and load were left unchanged. When prompted, the Masscomp data acquisition system collected all of the temperature, pressure, engine condition and emissions data. Gas chromatograph measurements would be taken at this time.

Without adjusting any of the engine conditions, the quench gas injection system was turned on. The addition of quench gas to the exhaust system required that the exhaust back pressure be adjusted to maintain ½ inch Hg over atmospheric. Data collection proceeded once the exhaust gas temperature and emissions levels stabilized. A GC sample would be taken at this time.

Once the data was taken, dilution air was added to the exhaust runner in addition to the quench gas being injected. As before, only the exhaust back pressure was adjusted to maintain ½ inch Hg over atmospheric. Data was collected once the emissions levels reached steady-state. This same procedure was repeated with the quench gas injection system shut off but with the dilution air continuing to flow.

Data collection under these four exhaust conditions constituted the procedure followed during the experiment and required for data analysis.

3.4 Data Analysis

The injection of quench gas into the exhaust system diluted the HC emissions. Retrieval of the undiluted emissions was necessary before any analysis could be made.

3.4.1 Correction of HC Emissions Due to Quench Gas Injection

Direct emissions measurements were used to quantify the mass flow rate of quench gas injected into the exhaust system. The operating procedure outlined in Figure 3.3-1 also indicates the relevant measurements made at each step. Under normal exhaust conditions, the HC and CO_2 concentrations were significant. During quench gas injection, the critical measurement was the diluted, total HC concentration. The next two steps, which had quench gas plus air and air only as the respective exhaust gas diluents, were used only to quantify the mass flow rate of quench gas injected at step two. The CO_2 concentrations were significant under both of these exhaust conditions. Had the CO_2 emissions analyzer been equipped to accommodate concentrations as large as 60% by volume, the quench gas mass flow rate could have been quantified directly from the CO_2 measurements made at steps one and two. Because the emissions range was not large enough, steps three and four were added; air added in step three diluted the CO_2 emissions to keep them on scale so they could be read off the analyzer; step four was added to quantify the mass flow rate of dilution air.

Given the measurements from each of these four steps, the basic approach to evaluating the quench gas mass flow rate was as follows: the change in CO_2 concentration from steps three to four quantified the air mass flow rate. Given the air mass flow rate, the CO_2 concentration at step three could then be corrected for air dilution. When this adjusted CO_2 was used in conjunction with the CO_2 concentration measured at step one, the quench gas mass flow rate could then be calculated. The total HC concentration measured at step two was then corrected for quench gas dilution. By examining the

change in O_2 concentration from steps one to two, the quench gas mass flow rate was verified. However, this verification was valid only under lean engine conditions, while the four step procedure extended to all equivalence ratios.

The correction factor resulting from the CO_2 measurements made at steps one, three and four was the following:

$$\frac{(x_{HC})_{Quench,wet}}{(x_{HC})_{Corrected,wet}} = \frac{1-(x_{CO_2})_{Quench,wet}}{1-(x_{CO_2})_{Exhaust,wet}} \qquad \text{(Eqn. 3.4-1)}$$

where $(x_{HC})_{Quench,wet}$ and $(x_{CO_2})_{Quench,wet}$ are the quench gas diluted HC and CO_2 mole fractions, $(x_{HC})_{Corrected,wet}$ is the HC mole fraction corrected for quench gas dilution, $(x_{CO_2})_{Exhaust,wet}$ is the CO_2 mole fraction under normal exhaust conditions. The subscript "wet" denotes engine-out concentrations from which the water vapor has not been removed. Note that the wet CO_2 values in the above expression are calculated from the "dry" CO_2 measurements in which the water vapor has been removed. A detailed development of the correction factor, which includes a correction for water vapor extraction, is outlined in Appendix B. Equation 3.4-1 could be used to correct all quench gas diluted emissions measured and not just the HC emissions. The correction factor was applicable at all equivalence ratios because it was based on relative CO_2 concentrations.

3.4.2 Data Analysis Approach

Having corrected the HC emissions for dilution due to quench gas injection, the emissions data available for analysis are illustrated in Figure 3.4-1. HC_1, HC_2 and HC_0 represent the cylinder exit, port exit and pre-catalyst runner exit HC emissions, respectively. They were obtained by injecting of quench gas just behind the exhaust valve, by injecting of quench gas at the port exit and running under normal engine exhaust conditions, respectively.

HC_1, HC_2 and HC_0 can refer to either the total HC emissions or an individual HC species from the speciated data.

Data analysis involved looking at the total or speciated HC emissions at the points in Figure 3.4-1 and the HC oxidation levels between the above points along the exhaust system. To evaluate the extent of HC oxidation, the following expressions were defined:

$$\Delta f_{HC}(overall) = \frac{(HC_1 - HC_0)}{HC_1} \qquad \text{(Eqn 3.4-2)}$$

$$\Delta f_{HC}(port) = \frac{(HC_1 - HC_2)}{HC_1} \qquad \text{(Eqn. 3.4-3)}$$

where Δf_{HC}(overall) and Δf_{HC}(port) represent the fractions of overall and port HC oxidation, respectively. Note that the overall fraction could not be broken down into port and runner fractions unless data was taken using the port exit injector.

3.5 Consistency of HFID and GC Measurements of HC Emissions

Both the HFID and GC were used to measure the total HC emissions. When measured under the same engine operating condition, the results from the two techniques were reliable if and only if the results were comparable. When the total HC emissions and overall fraction reduced were plotted for each technique, the results indicated that the HFID and GC measurements were within 5-10% of one another for all the fuels tested.

TABLE 3.1-1 Baseline Engine Operating Condition

Engine Speed	IMEP	Spark Timing	Φ	Coolant Temperature
1500 RPM	3.8 bar	MBT	0.9	88 °C

TABLE 3.1-2 Fuels Tested at the Baseline Operating Condition

Fuel	Formula (Phase)	Molecular Structure
Methane	CH_4 (g)	Alkane
Ethane	C_2H_6 (g)	
Propane	C_3H_8 (g)	
n-Butane	C_4H_{10} (g)	
Iso-octane	C_8H_{18} (l)	
Ethene	C_2H_4 (g)	Alkene
Toluene	C_7H_8 (l)	Aromatic
Gasoline (RON=91)	$C_nH_{2.02n}$ (l)	Complex

TABLE 3.1-3 Engine Parameters Swept About the Baseline Condition

Engine Speed (RPM)	IMEP (bar)	Spark Timing	Φ	Coolant Temperature (°C)
830	2.9	6 deg. retard from MBT	0.9	27
1000	3.2	12 deg. retard from MBT	1.0	60
2000	4.5		1.1	74
2500	5.5			
	6.0			
	6.5			

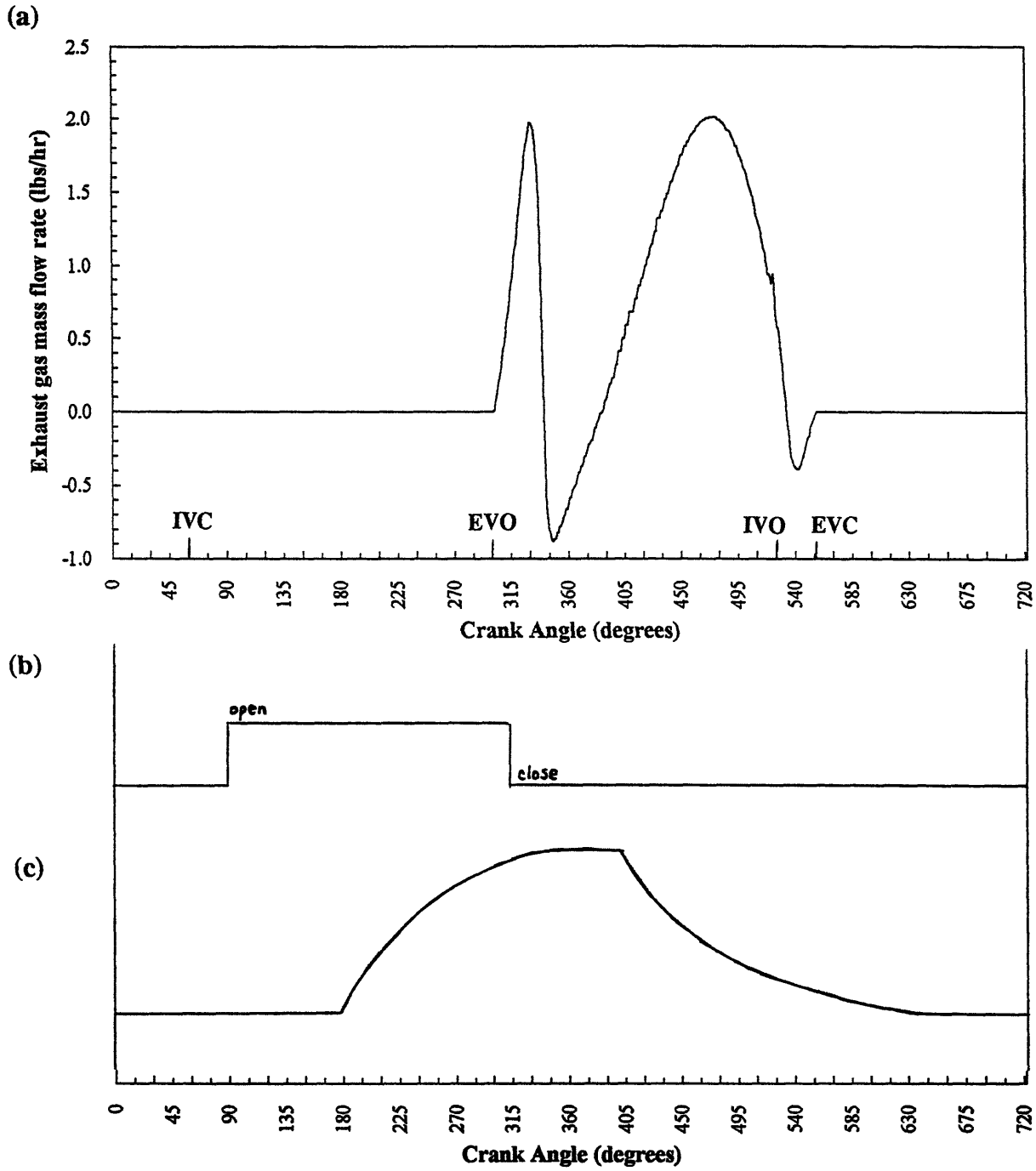

FIGURE 3.2-1 Optimization of the quench gas injection timing for the baseline operating condition. Optimization requires knowing the (a) exhaust gas mass flow rate and valve timing, (b) signal from the controller, which indicates both the length and start of injection, and (c) pressure trace downstream of the solenoid, which indicates the approximate delivery of quench gas to the exhaust system.

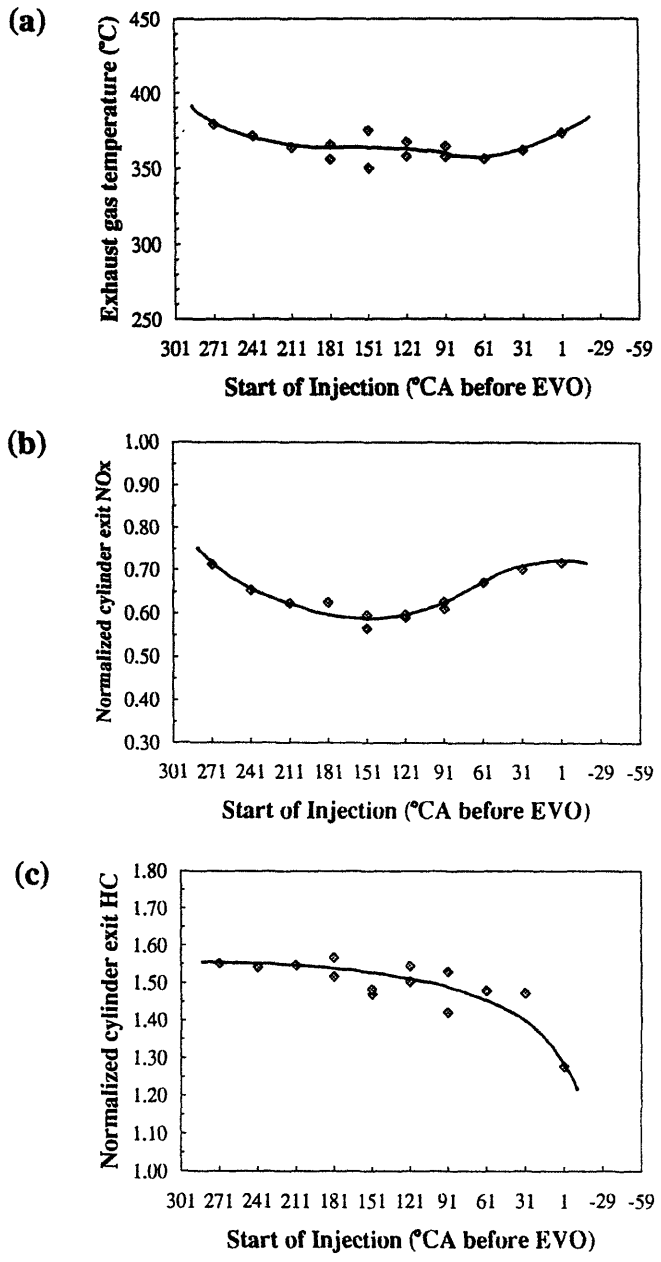

FIGURE 3.2-2 Optimization of the start of injection based on the response of the (a) exhaust gas temperature during quench gas injection, (b) normalized cylinder exit NO_x and (c) normalized cylinder exit HC.

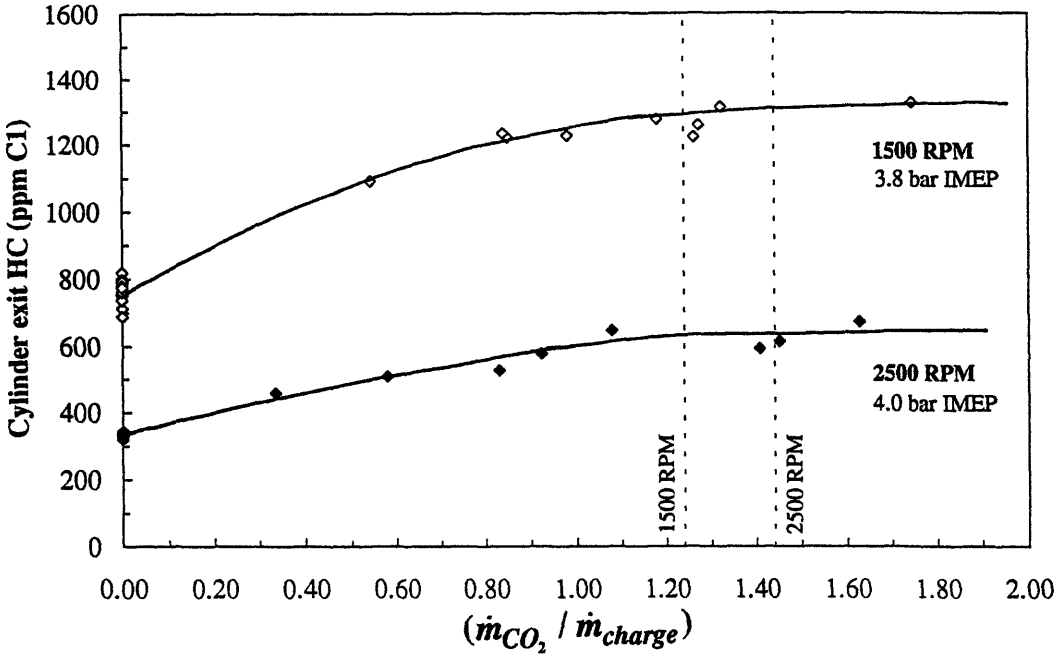

FIGURE 3.2-3 Check for sufficient quenching at the cylinder exit based on the response of the HC emissions to increasing mass flow rates of quench gas. Optimum quench gas flow rates for 1500 and 2500 RPM are indicated.

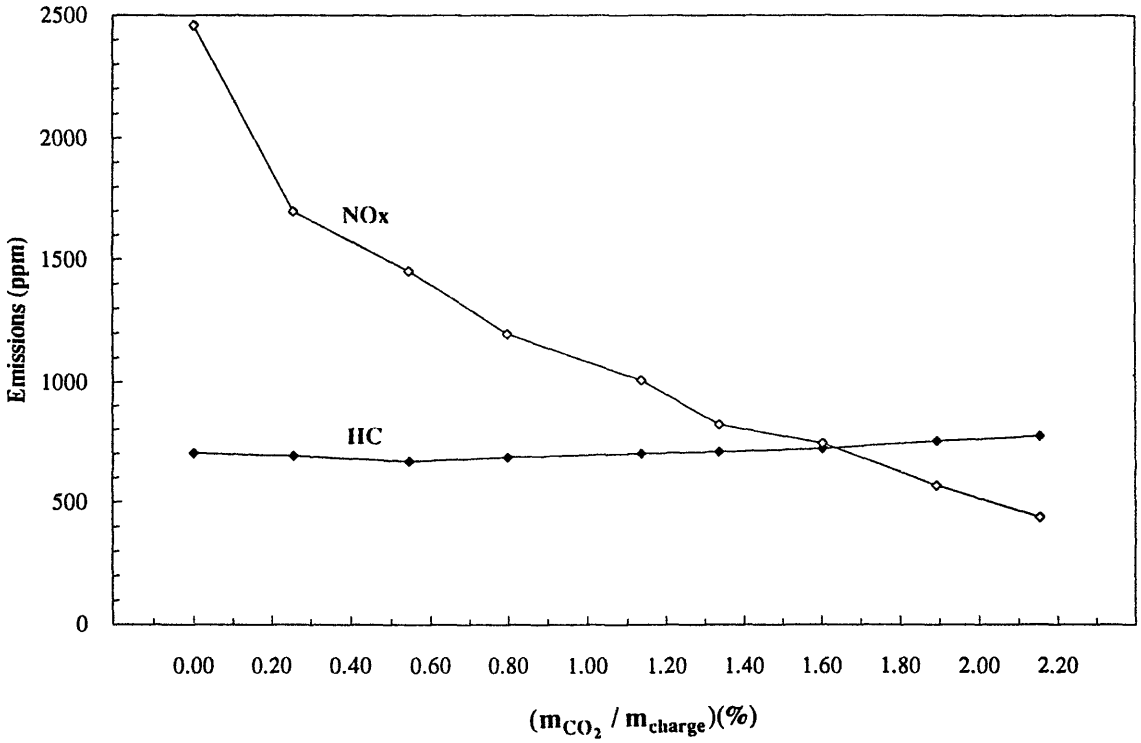

FIGURE 3.2-4 Sensitivity of engine emissions to the addition of CO_2 mass in the intake charge.

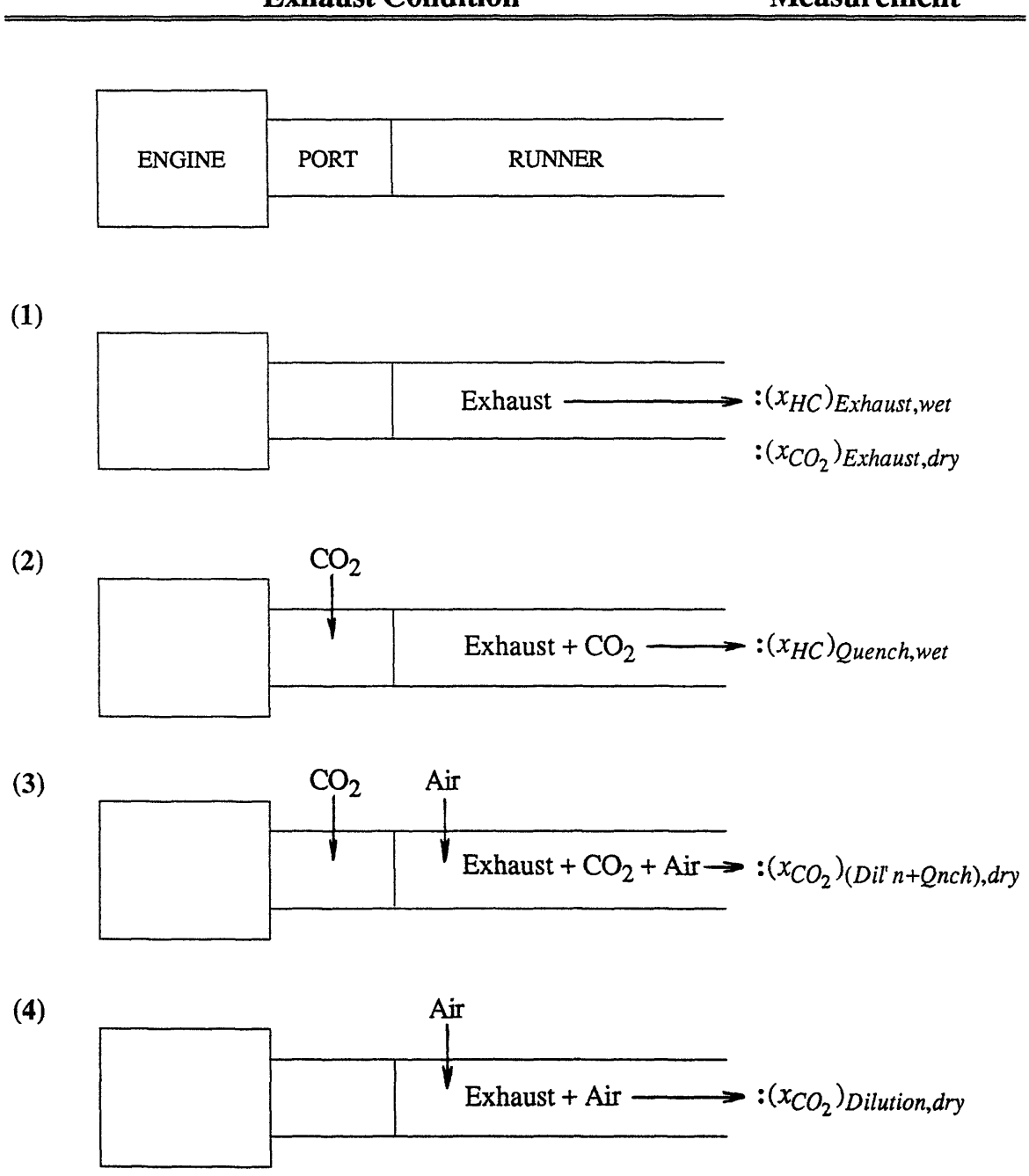

FIGURE 3.3-1 Experimental procedure used to obtain measurements necessary for correcting the emissions for dilution due to quench gas injection before analysis.

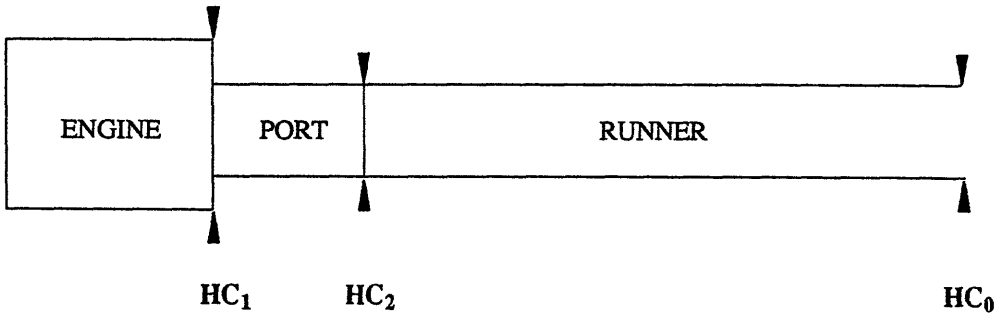

FIGURE 3.4-1 Physical representation of where data is available following correction of the HC emissions for dilution due to quench gas injection; HC_1, HC_2 and HC_0 represent the cylinder, port and runner exit HC emissions, respectively.

Chapter 4

Fuel Effects at Fixed Operating Condition

4.1 Total HC Emissions

The total HC emissions (in ppm C_1) emitted at the baseline operating condition for the fuels listed in the fuel composition matrix (Table 3.1-2) are shown in Figure 4.1-1. Cylinder exit (a), port exit (b) and pre-catalyst runner exit (c) HC emissions are indicated for the fuels. Port exit (b) HC emissions are absent for ethane, n-butane and ethene as injector (2) data was never obtained. As a result, only the overall fraction of HC reduced, Δf_{HC}(overall), could be determined. The emissions indices for the fuels (Figure 4.1-2) emphasize the difference in in-cylinder effects on the gaseous and liquid fuels. For the same inducted mass of fuel, the gaseous fuels generate lower unburned HC mass (0.015 to 0.05) than the liquid fuels (0.17 to 0.22).

The cylinder exit HC emissions range from 460 ppm C_1 for ethene to 3400 ppm C_1 for toluene. With the exception of methane, the HC emissions from the alkane fuels increase as with increasing molecular weight. When grouped according to phase, the

liquid fuels (gasoline, iso-octane and toluene) have significantly higher HC emissions than the gaseous fuels. These observations in themselves do not explain the large differences in total cylinder exit HC emissions between the fuels. Possible explanations include differences in HC oxidation rates, oil layer mechanism, and molecular diffusivity of the HC. Ranking the fuels according to the time for 50% of the total HC reactions to occur yields $C_2H_6 < C_3H_8 \cong n-C_4H_{10} < i-C_8H_{18} < C_7H_8 < CH_4$ [8]. Fuels such as ethane and ethene, which have the lowest total HC emissions, are highly reactive compared with stable fuel species like methane and toluene. Despite their relatively slow oxidation rates, methane and toluene cylinder-exit HC emissions (1150 and 3400 ppm C_1, respectively) are dramatically different. By themselves, oxidation rates do not resolve the emissions differences between the fuels.

The oil layer absorption/desorption mechanism contributes to nearly 20% of the total engine-out HC emissions [3]. This effect is insignificant for fuels below C_6 because they are not very soluble in the lubricant [9]. This applies to methane, ethane, ethene propane and n-butane. Aromatics are more soluble than alkanes and alkenes with the same carbon number [10]. Less fuel is stored in the lubricant during compression and combustion for the lower solubility HC fuels than for the higher solubility fuels. As a result, they are desorbed or released earlier in the cycle. This allows more time for in-cylinder oxidation when the bulk gas temperature is higher and the reaction rates are faster [11]. The oil layer mechanism partially accounts for the emissions difference between the gaseous (C_1-C_5) fuels and the liquid fuels.

Diffusivity of the fuel molecules is yet another contributor. In relation to the crevice and oil layer HC formation mechanisms, the lower molecular weight fuels will diffuse out of the boundary layer faster. This gives them more time to mix and react with the bulk gases, resulting in increased levels of in-cylinder oxidation and lower HC emissions at the cylinder exit [4].

Continuing through the exhaust system, the gas leaving the port (b) experiences a substantial drop in total HC emissions. Despite the runner's length (1.8 m), the drop in HC emissions at the runner exit (c) is minimal.

The fraction of HC reduced for the different fuels at the same baseline operating condition is shown in Figure 4.1-2. For ethane, n-butane and ethene port exit HC emissions were not measured and, as a result, the port/runner oxidation could not be separated; for these fuels the only value indicated is the overall port/runner fraction reduced. As for the remaining fuels, their port and runner fractions were separated. Consider first the overall fraction of HC reduced, which are the maximum values indicated for each fuel. Oxidation levels for all fuels fall within 40±5%. This indicates that exhaust port/runner HC oxidation is fuel independent despite the large HC emissions differences seen earlier. This result suggests that HC oxidation in the exhaust port/runner is "mixing dominated" as opposed to mixing controlled due to the port and runner results. Results clearly indicate that a majority of the HCs are reduced in the port (30-35%), while a small fraction is reduced in the runner (5-10%). The residence times in the port and runner at the baseline condition are estimated at 5 and 144 msec, respectively. Stratification of the HC emissions entering the port [5] and similar fractions reduced for the fuels tested suggest that oxidation within the port is mixing controlled. Although the runner is quite long and there is adequate time for mixing and oxidation to occur, the low exhaust gas temperatures imply that runner oxidation is chemistry controlled. The overall oxidation then becomes a "mixing dominated" process.

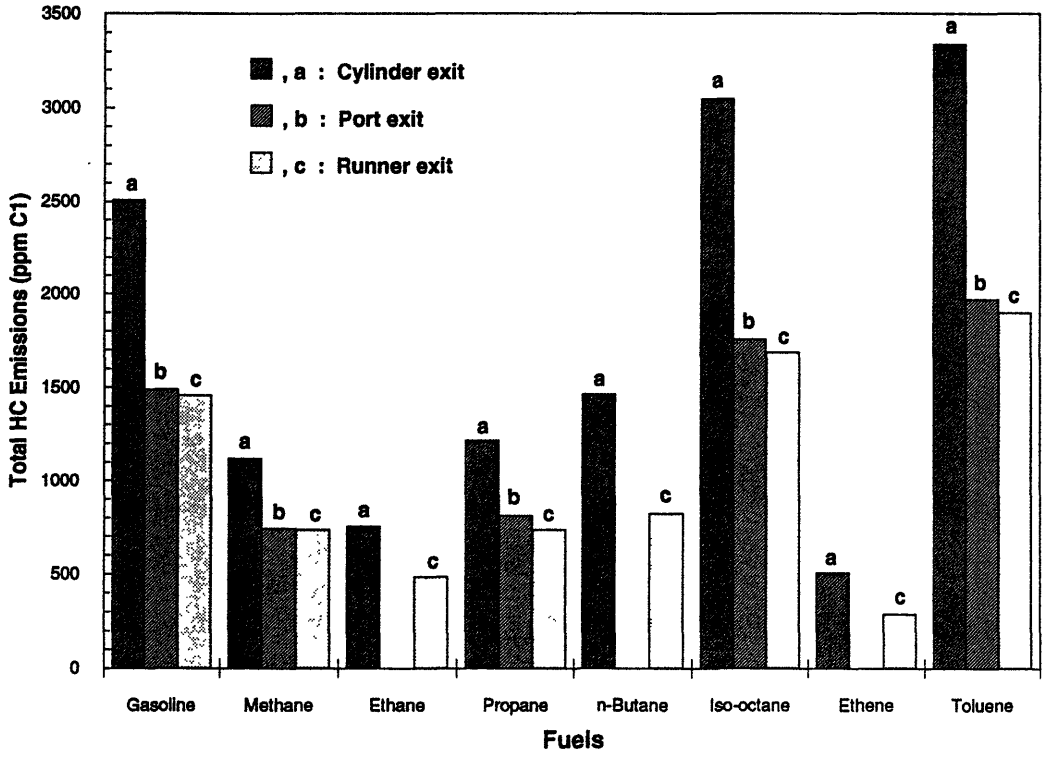

FIGURE 4.1-1 Total HC emissions at the cylinder, port and runner exits for the different fuels.

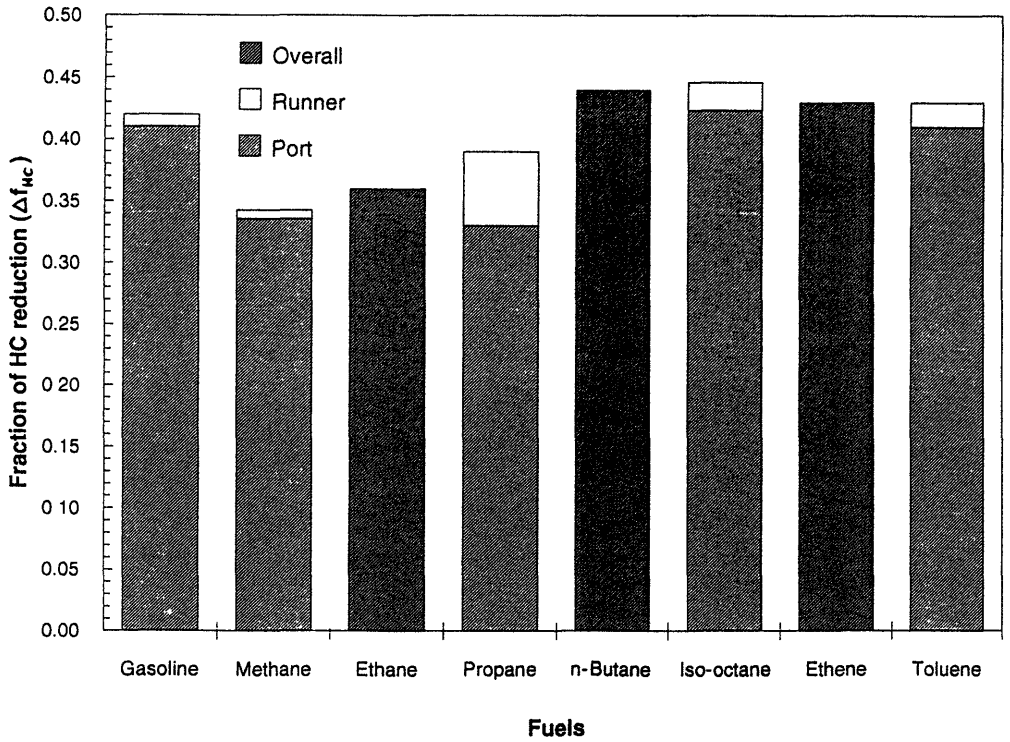

FIGURE 4.1-2 Emissions indices at the cylinder, port and runner exits for the different fuels.

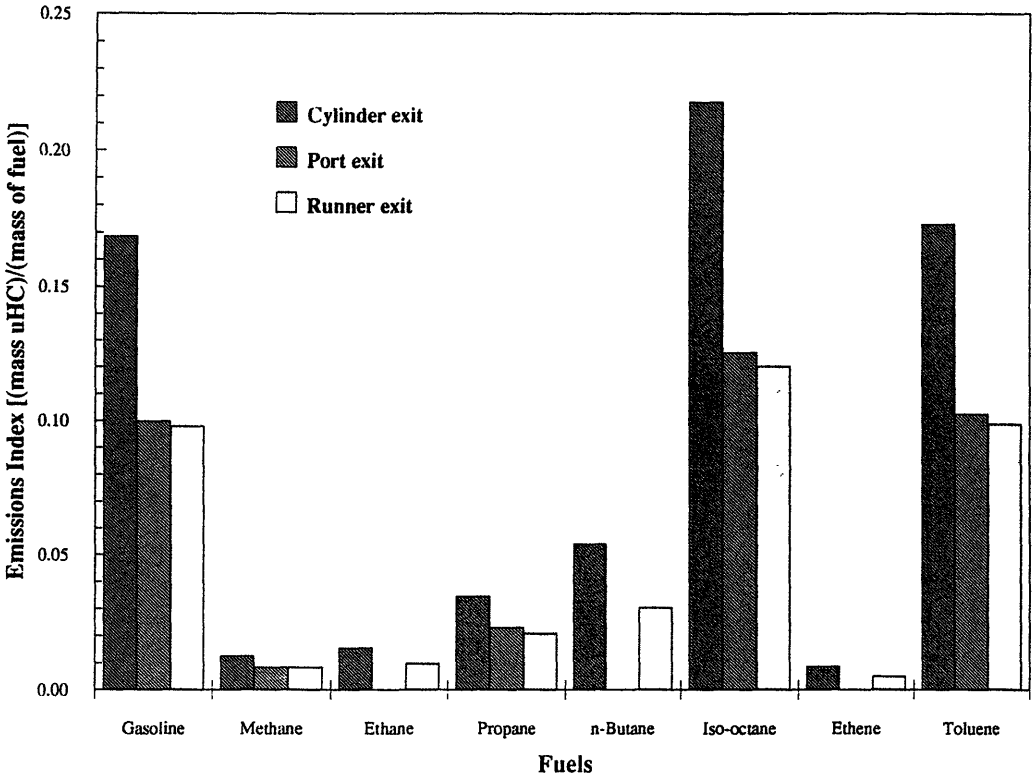

FIGURE 4.1-3 HC reduction (as a fraction of cylinder-out value) in the exhaust port/runner system. Measurements at the port exit were not made for ethane, ethene or n-butane fuels.

Chapter 5

Speciated Results

5.1 Fuel and Non-fuel Species

The HC emitted at the baseline operating condition by the different fuels were speciated. This enabled the HC emissions from the pure component fuels to be separated into fuel and non-fuel species. Cylinder exit (a), port exit (when available) (b) and pre-catalyst runner exit (c) results appear in Figure 5.1-1. Unburned fuel is the major cylinder-out species in every case. There is a substantial drop in the fuel species concentration at the port exit. The non-fuel species concentrations, however, do not change significantly from cylinder exit to port exit to reflect the substantial HC oxidation. It is plausible that the oxidation of the non-fuel species may have been replenished by the partial oxidation and decomposition of the fuel species. Fuel species concentrations also decrease in the runner though at much lower levels.

Despite the large overall decrease in fuel species concentration from the cylinder exit to the runner exit, Figure 5.1-2 shows that the fuel species contribution to the total

HC emissions (given as a percent of the total) remains significant. Methane, ethene and toluene distinctively have the highest unburned fuel contributions. The cylinder exit fuel contribution for methane and ethene are 94% and 93%, respectively. While the contribution remains constant at 95% and 94% for methane at the port and runner exits, respectively, it drops slightly to 90% for ethene at the runner exit. For toluene, however, there is a small but significant decrease in the contribution of fuel to the total HC emissions. Decreasing from 89% to 85% and then to 82% at the cylinder, port and runner exits, respectively, indicates ongoing oxidation. The unburned fuel contribution for the remaining non-methane alkane fuels (ethane, propane, n-butane and iso-octane) is all-around lower and undergoes dramatic changes compared to methane, ethene and toluene. At the cylinder exit, the fuel contributions range from 61-69% and decrease by 15-18% of the total HC emissions at the runner exit. In effect, the unburned fuel contribution remains independent of carbon number for the non-methane alkane fuels. For propane and iso-octane, the contributions at the cylinder, port and runner exits are 62%, 55% and 47% and 62%, 56% and 45%, respectively. The decrease across the runner in particular is indicative of significant reaction within the runner even at the baseline condition.

5.2 Species Distribution

The decrease in the percentage contribution of unburned fuel to the total HC emissions is coupled with an increase in the percentage contribution of the intermediate combustion products. HC species distributions are pictured in Figures 5.2-1 and 5.2-2 for the fuels tested at the baseline operating condition. Distributions are represented at the cylinder exit (a), port exit (when available) (b) and runner exit (c).

The small amount of non-fuel species present for methane are C_2 products of recombination. As for ethene, methane and ethyne are the dominant products. As

toluene's overall fuel contribution decreases from 89% to 82%, it is accompanied by an overall increase from 2.3% to 3.2% for ethyne, 1.2% to 4.6% for methacrolein and 3.5% to 5.2% for benzene, respectively. Although these contributions are small compared to toluene's, their formation is evidence that reaction continues throughout the port/runner system.

Species distributions for the non-methane alkane fuels can be found in Figure 5.2-2. These fuels have the most significant changes in non-fuel species contribution and species distribution. For example, for ethane the overall fuel contribution decreases from 69% to 54% while the fraction of ethene increases from 27% to 41%. Consider propane, whose dominant intermediate species include ethene and propene. As the fuel species contribution decreases in the cylinder, port and runner exit (62%, 55% and 47%, respectively), ethene contributes 18%, 23% and 29%, respectively, while propene contributes 10%, 13% and 15%. N-Butane's dominant intermediates are also ethene and propene; their contributions to the total HC emissions at the cylinder and runner exits are identical to propane's ethene and propene contributions. Propene and iso-butene contribute the most to iso-octane's intermediates. As the fuel species contribution decreases in the cylinder, port and runner exit (62%, 56% and 45%, respectively), propene contributes 6%, 7.3% and 9.3%, respectively, while iso-butene contributes 16%, 19% and 24%, respectively.

Monitoring changes in species distribution across the port and runner is critical because there exists the potential to generate species that are highly reactive in forming atmospheric photochemical smog. Alkenes and aldehydes have a much higher smog forming potential than do alkanes. From the species distributions, combined ozone reactivity factors [2] were calculated for the cylinder, port and runner exit HC emissions using the maximum incremental reactivity values proposed by the California Air Resources Board (CARB) in 1992 [12]. Results appear in Figure 5.2-3. Ethene has the highest reactivity because it has the highest percentage contribution of alkenes in the exhaust.

Ethene and toluene reactivities remain constant throughout the exhaust system because the significant unburned fuel contribution remains fairly constant throughout the port/runner with negligible formation of reactive species.

The reactivities of the non-methane alkane fuels increase with increasing carbon number. A summary of the overall reactivity formation factors appears in Table 5.2-1. It indicates that the increase in combined ozone reactivity from the cylinder exit to the runner exit is effectively the same despite the reactivity differences between the fuels. Propane and iso-octane results indicate significant reactivity increases on both the port and runner. Cylinder, port and runner exit combined ozone reactivities for propane and iso-octane are 2.69, 3.21 and 3.82 g O_3/g NMOG and 3.33, 3.81 and 4.67 g O_3/g NMOG, respectively. The reactivities increase in the port and runner by factors of 1.19 and 1.23 for propane and 1.14 and 1.26 for iso-octane. Though only 5-10% of the overall reduction in total HC emissions occurs in the exhaust runner, the runner factors indicate that a significant amount of species conversion is taking place in the runner. A majority of the conversions within the port and runner are from the alkanes to the light alkenes, which account for the significant increase in ozone reactivity. For propane, the percentage of alkane contribution (which includes the unburned fuel contribution) decreases from 67% at the cylinder exit to 61% at the port exit and 52% at the runner exit. This is accompanied by an increase in alkene contribution from 29% at the cylinder exit to 36% at the port exit and 44% at the runner exit. Similar results are observed for iso-octane.

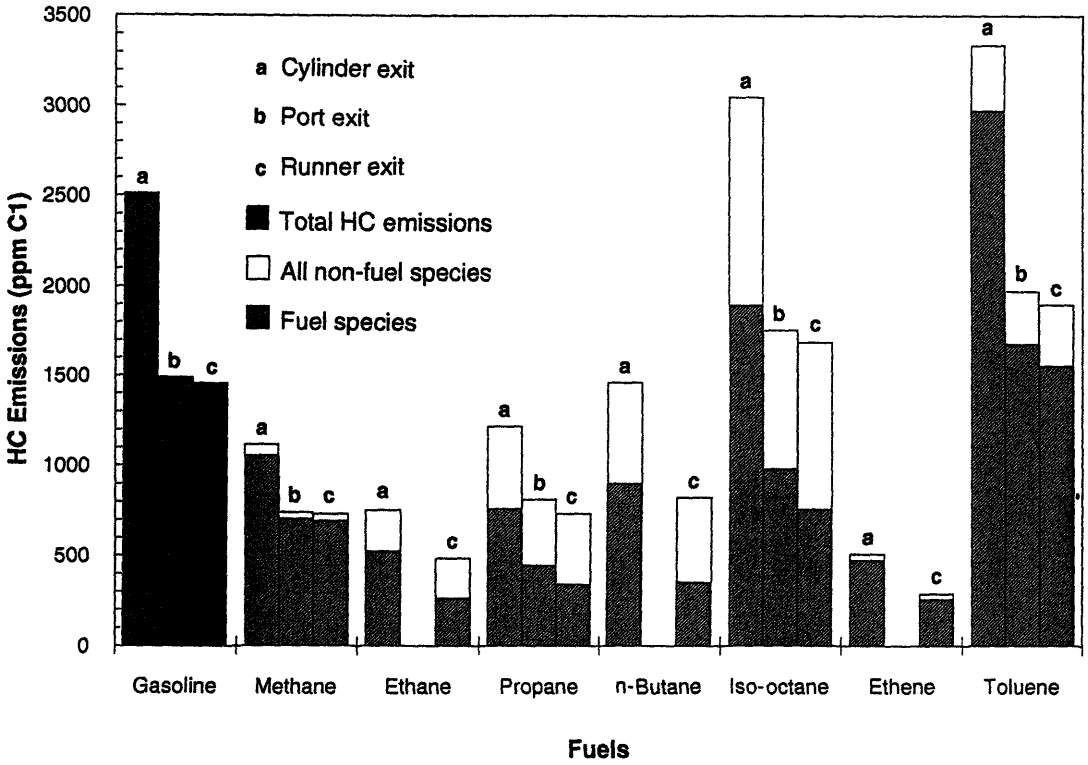

FIGURE 5.1-1 Fuel and non-fuel species HC emissions at the cylinder, port and runner exits for the different fuels. Gasoline was not presented this way.

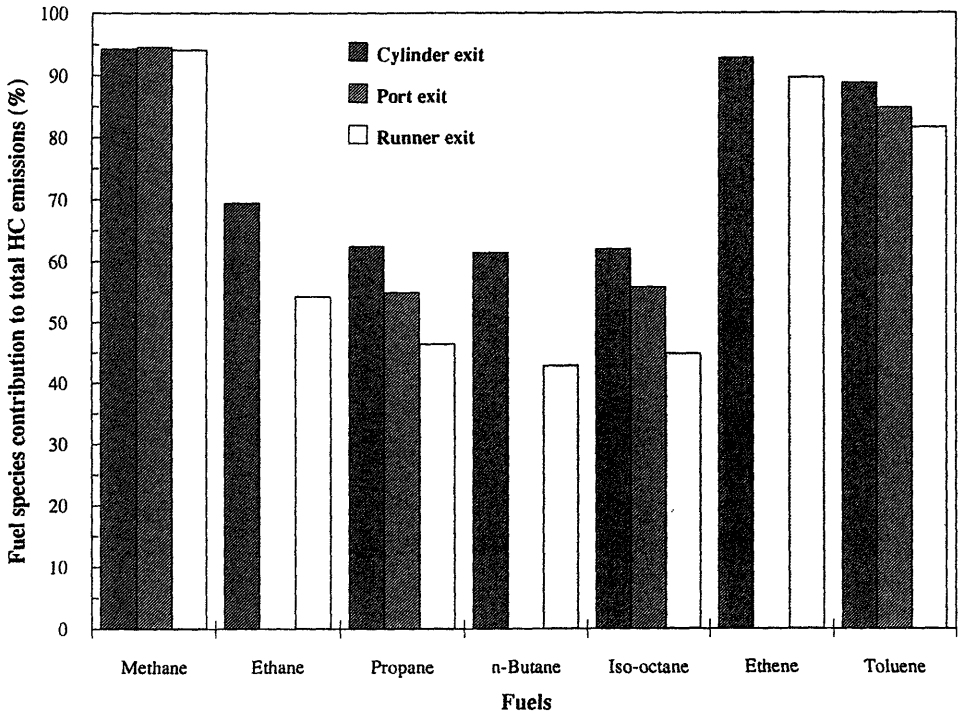

FIGURE 5.1-2 Fuel species concentration shown as a percentage of the total HC emissions at the cylinder, port and runner exits for the different fuels.

TABLE 5.2-1 Summary of the Overall Reactivity Formation Factors

Fuels	NMOG Reduction (%)			MIR Index (g O3/g NMOG)			Change in MIR Index (by factor of)			Reduction in MIR of exhaust		
	port	runner	overall	cylinder exit	port exit	runner exit	port	runner	overall	port	runner	overall
Ethane			35.0	2.087		3.078			1.475			4.2
Propane	32.1	7.7	39.8	2.688	3.205	3.822	1.192	1.229	1.422	19.0	-4.7	14.4
n-Butane			44.3	3.287		4.476			1.362			24.1
Iso-octane	42.6	1.3	43.9	3.331	3.805	4.670	1.142	1.260	1.402	34.4	-13.1	21.4
Ethene			42.0	7.054		6.918			0.981			43.2
Toluene	42.6	0.0	42.6	2.662	2.703	2.719	1.015	1.006	1.021	41.7	-0.4	41.4

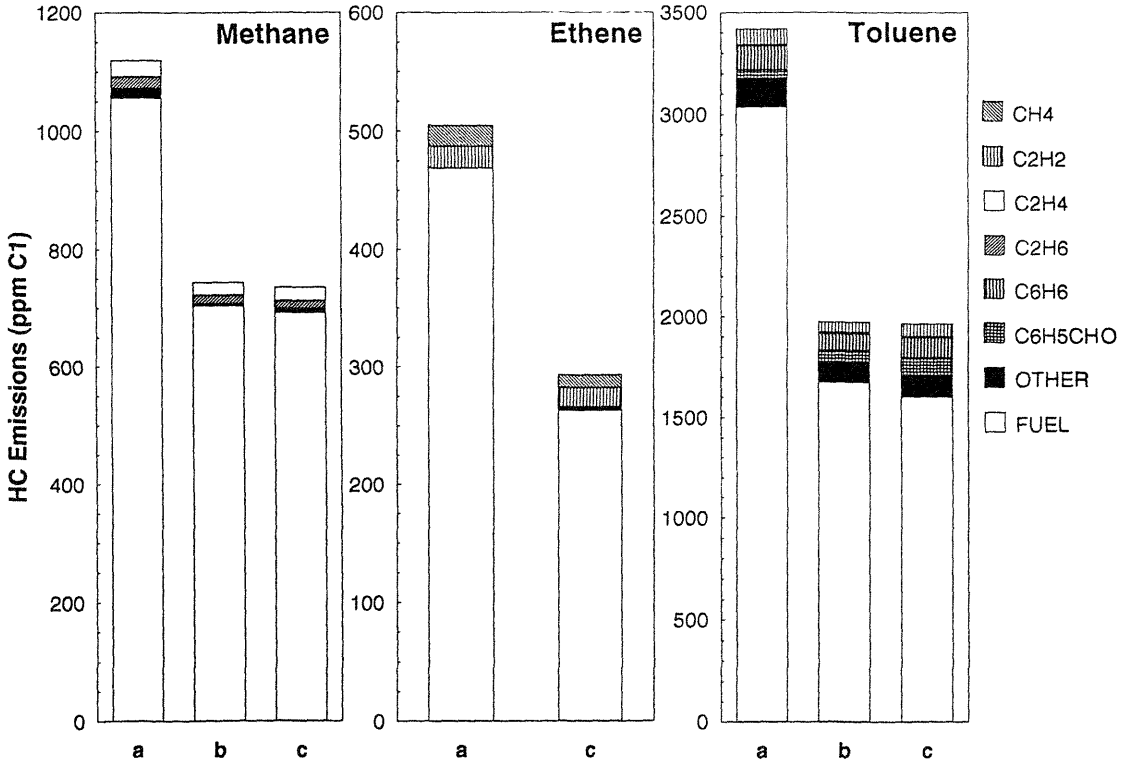

FIGURE 5.2-1 Speciated HC emissions for methane, ethene and toluene at the cylinder exit (a), port exit (b) and runner exit (c).

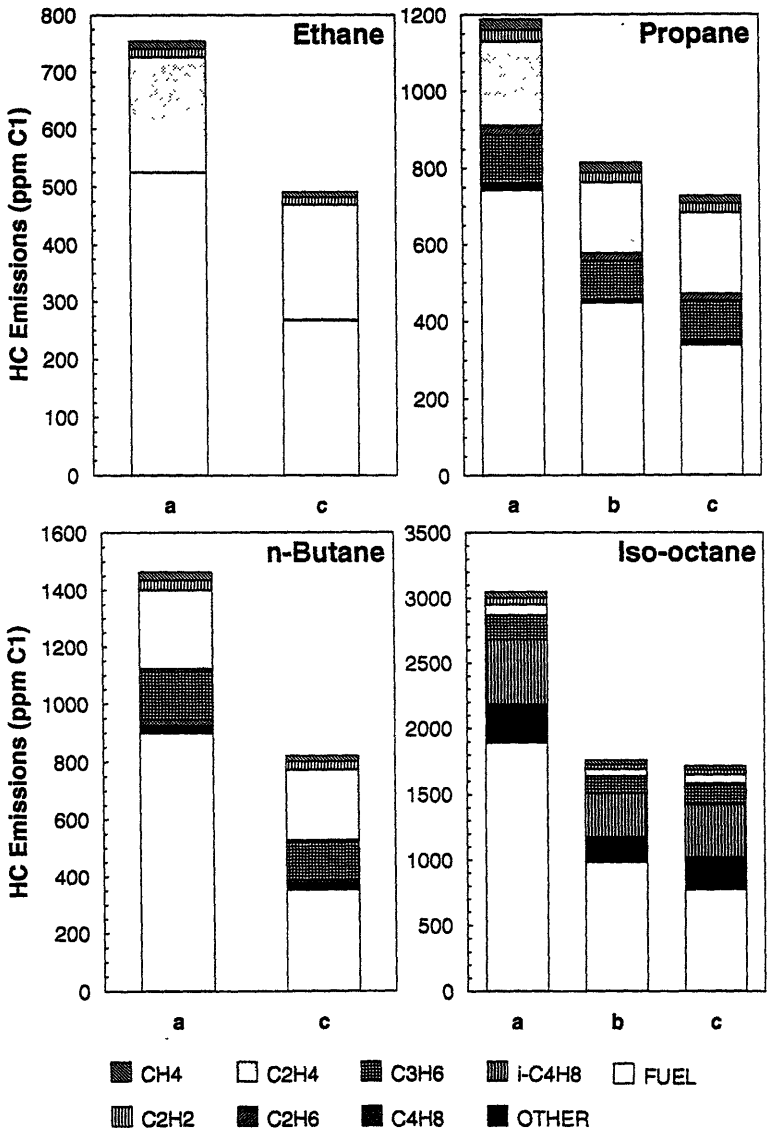

FIGURE 5.2-2 Speciated HC emissions for ethane, propane, n-butane and iso-octane at the cylinder exit (a), port exit (b) and runner exit (c).

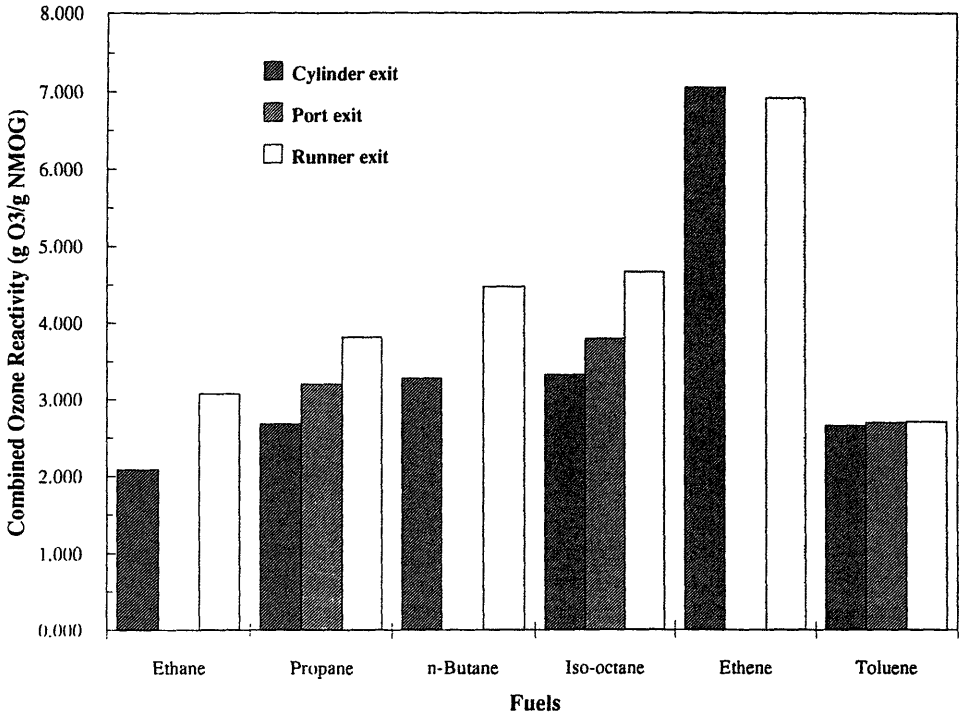

FIGURE 5.2-3 Combined ozone reactivity at the cylinder, port and runner exits for the non-methane fuels.

Chapter 6

Dependence of Exhaust Oxidation to Operating Condition with Different Fuels

To investigate the effect of engine parameters on the extent of HC oxidation in the exhaust port/runner system, several single parameter sweeps were made about the baseline operating condition. The parameters of interest included engine speed, load (IMEP), spark timing, equivalence ratio and coolant temperature. A complete data set was run for gasoline (where stoichiometry was used for the baseline equivalence ratio instead of 0.9) and partial sets were run for propane and iso-octane. Because the sweeps were repeated using different fuels, the joint dependence of exhaust system oxidation to operating condition and fuel type was also considered. A small set of experiments in which parameters were varied jointly were also completed to investigate the interactions between engine parameters and their effect on HC oxidation As hydrocarbon oxidation is thought to be governed by the exhaust gas temperature, O_2 concentration, mass flow rate and port residence time [7], the results will be analyzed in this light.

6.1 Engine Speed

Engine speed was varied from 1000 to 2500 rpm while maintaining the baseline load, spark timing, Φ and coolant temperature settings. The effect of engine speed on exhaust gas temperature and O_2 concentration are shown in Figures 6.1-1(a) and (b), respectively. With the same load at higher speeds the significance of any heat transfer effect is greatly reduced due to the higher overall mass flow rate and the lack of time. Therefore, as engine speed increases, the exhaust gas temperature increases.

The gasoline results were obtained at stoichiometric condition, while iso-octane and propane results were under lean conditions. This explains why gasoline has a lower O_2 concentration and a higher exhaust temperature. As engine speed increases, the O_2 concentration decreases somewhat.

The effect of engine speed on the cylinder exit HC emissions and the overall fraction reduced are shown in Figures 6.1-1(c) and (d), respectively. For gasoline, as the engine speed increases, the cylinder-exit HC emissions drop from 3300 ppm C_1 at 1000 rpm to 1400 ppm C_1 at 2500 rpm partly due to the increased bulk gas temperature during expansion and partly due to a reduced oil layer absorption/desorption mechanism because of higher liner temperatures [13]. The overall fraction reduced drops from 0.43 at 1000 rpm to 0.35 at 2000 rpm and then significantly to 0.21 (approximately) at 2500 rpm. The scatter at 2500 rpm is due to repeated runs after cleaning of the combustion chamber by running many high speed, high load cases before acquiring the data. Iso-octane and propane cylinder-exit HC emissions (Figure 6.1-1(c)) also decrease in concentration with increasing engine speed. The cylinder-exit HC emissions for both fuels are reduced approximately by a factor of 0.5, independent of rpm. The HC reduction for these fuels are different than those for gasoline. Part of the difference lies in the fact that iso-octane and propane were run lean.

6.2 Load

Load (IMEP) was varied from 2.8 to 6.5 bar while maintaining the baseline engine speed, spark timing, Φ and coolant temperature settings. The effect of load on exhaust gas temperature and O_2 concentration are shown in Figures 6.2-1(a) and (b), respectively. As load increases, the exhaust gas temperature increases modestly, and the O_2 concentration remains virtually unchanged for the different fuels. Recall that gasoline was run at stoichiometric but iso-octane and propane were lean.

The effect of load on the cylinder exit HC emissions and the overall fraction reduced are shown in Figures 6.2-1(c) and (d), respectively. As the load increases from 2.8 bar to 6.5 bar IMEP, the cylinder-exit HC emissions decrease from 3000 ppm to about 2200 ppm C_1. As Figure 6.2-1(d) indicates, gasoline HC oxidation is about 0.42 at 3 bar and reduces to 0.10 at 6.5 bar. The iso-octane cylinder-exit HC emissions follow the same trend as the gasoline data. Compared to gasoline, iso-octane HC oxidation remains significant (38%) even at high load (5.4 bar).

6.3 Spark Timing

Spark timing was retarded 6 and 12 degrees from MBT while maintaining the baseline engine speed, load, Φ and coolant temperature settings. The effect of spark timing on exhaust gas temperature and O_2 concentration are shown in Figures 6.3-1(a) and (b), respectively. As the spark timing is retarded, the exhaust gas temperature increases modestly, while the O_2 concentration remains virtually unchanged for the different fuels.

The effect of spark timing on the cylinder exit HC emissions and overall fraction reduced are shown in Figures 6.3-1(c) and (d), respectively. Going from MBT to 12 degrees retarded, gasoline's cylinder exit HC emissions diminish from 2600 ppm C_1 to

2100 ppm C_1. The overall fraction reduced increases from 0.37 to 0.48, respectively. Iso-octane and propane cylinder-exit HC emissions also decrease with spark retard. However, the oxidation results differ between the fuels. Iso-octane HC oxidation is almost independent of retarded spark timing at a value of 45%. Propane oxidation at MBT is comparable to gasoline at 37% but rises to 56% at 12 degrees retarded. The differences between the fuels cannot be explained by the O_2 availability and exhaust temperature increase alone; the differences may be chemistry related.

6.4 Equivalence Ratio

Equivalence ratio was varied from 0.9 to 1.1 while maintaining the baseline engine speed, load, spark timing and coolant temperature settings. The effect of equivalence ratio on exhaust gas temperature and O_2 concentration are shown in Figures 6.4-1(a) and (b), respectively. The exhaust gas temperature is hottest around stoichiometric and decreases when the mixture gets lean or rich. As the charge is enriched, the O_2 concentration decreases dramatically. At equivalence ratios of 0.9 and 1.0 there is substantial O_2 available for oxidation.

The effect of equivalence ratio on the cylinder exit HC emissions and the overall fraction reduced are shown in Figures 6.4-1(c) and (d), respectively. At Φ=0.9, gasoline and iso-octane emissions begin to increase due to incomplete combustion. At richer mixtures the increase is even more pronounced due to the lack of O_2 and high temperatures for post-combustion burn up. Propane HC emissions are insensitive at lean conditions but respond as the other fuels do at rich conditions. Gasoline HC oxidation decreases from 42% at Φ=0.9 to 37% at Φ=1.0 and 33% at Φ=1.1. Despite the increase in HC emissions at rich conditions, the decrease in HC oxidation going from lean to stoichiometric is limited by the available O_2 despite to increasing exhaust gas

temperatures. The level of oxidation continues to drop as the charge is enriched due to both the lack of O_2 and decrease in exhaust temperature. From these results it is believed that O_2 concentration plays a significant role in governing HC oxidation levels. Propane's oxidation results are similar to gasoline's but remain consistently lower. Iso-octane's oxidation, on the other hand, appears to plateau around Φ=1.1 for reasons yet unknown.

6.5 Coolant Temperature

Coolant temperature was varied from 27 to 88 °C while maintaining the baseline engine speed, load, spark timing and Φ settings. The effect of coolant temperature on exhaust gas temperature and O_2 concentration are shown in Figures 6.5-1(a) and (b), respectively. The change in exhaust gas temperature is almost negligible. The O_2 concentration is independent of the coolant temperature increase.

The effect of coolant temperature on gasoline's cylinder exit HC emissions and the overall fraction reduced are shown in Figures 6.5-1(c) and (d), respectively. The cylinder-exit HC emissions decreased by a factor of 0.78, falling from 3350 ppm at 27 °C to 2600 ppm at 88 °C. As the coolant temperature increases, the cylinder wall temperature increases, which decreases the oil layer effect and thereby, reduces the cylinder exit HC emissions. The HC oxidation remains at 38% regardless of coolant temperature. That the level of HC oxidation does not change indicates that the coolant temperature affects the in-cylinder process rather than the exhaust process.

6.6 Joint Variations of Parameters

A small set of experiments in which parameters were varied jointly were completed to investigate the interactions between engine parameters and their effect on HC emissions and HC oxidation.

Figures 6.6-1(a)-(d) present iso-octane results for a multi-parameter sweep of speed and spark timing. Load, equivalence ratio and coolant temperature were fixed at the baseline conditions. The multi-parameter effect on exhaust gas temperature and O_2 concentration are shown in Figures 6.6-1(a) and (b), respectively. As spark timing is retarded, the exhaust gas temperature increases modestly for both 1500 and 2500 rpm. In turn the O_2 concentration decreases for 1500 rpm while remaining constant for 2500 rpm. The difference is due to the variation in load settings. The effect of the multi-parameter sweep on iso-octane's cylinder exit HC emissions and its overall fraction reduced are shown in Figures 6.6-1(c) and (d), respectively. As the spark timing is retarded the cylinder exit HC emissions decrease due to the increase in bulk gas temperatures; this increase also accounts for the emissions difference between the two engine speeds. The overall fraction reduced for 1500 rpm remains virtually constant at 43%. However, the results for 2500 rpm increase from 37% at MBT to 63% at 12 degrees retard.

Figures 6.6-2(a)-(d) present propane results for a multi-parameter sweep of equivalence ratio and spark timing. Load and coolant temperature were fixed at the baseline conditions, while engine speed was fixed at 2500 rpm. The multi-parameter effect on exhaust gas temperature and O_2 concentration are shown in Figures 6.6-2(a) and (b), respectively. As spark timing is retarded, the exhaust gas temperature increases to 710 °C from its initially high temperature of 665 °C at MBT timing. The initially high temperature is a result of operating at 2500 rpm. The temperature difference between Φ=0.9 and Φ=1.1 is negligible. As expected there is O_2 in the exhaust at Φ=0.9 but none at Φ=1.1. O_2 concentration remains constant over retarded timing. The effect of the

multi-parameter sweep on propane's cylinder exit HC emissions and its overall fraction reduced are shown in Figures 6.6-2(c) and (d), respectively. At Φ=1.1 the HC emissions decrease by a factor of 0.73; at Φ=0.9 they are reduced by a factor of 0.58. Despite the sizable decrease in cylinder exit HC emissions at Φ=1.1, the exhaust port/runner oxidation mechanisms appear to have shut off. This behavior is consistent over the range of retarded spark timing. In this case the lack of time and O_2 amidst the temperature increase blocks HC oxidation. On the other hand, oxidation under lean conditions increases significantly (40-70%) at 12 degrees retard. Available O_2 and high exhaust gas temperature boost oxidation at high speed.

Figure 6.6-3 presents iso-octane results for a quench plane sweep at 2500 rpm, 4.0 bar IMEP, 12 degrees retard, Φ=0.9 and $T_{coolant}$=88 °C. The cylinder, port and runner exit HC emissions are 1320, 1012 and 467 ppm C_1, respectively. This corresponds to port, runner and overall HC oxidation levels of 23%, 42% and 65%, respectively. Clearly high levels of HC oxidation can be achieved at a high speed, retarded and lean operating condition. Compared to the 5-10% runner oxidation levels achieved at the baseline operating condition, it is evident that O_2 availability along with dramatic increases in exhaust gas temperature can offset the reduction in port residence time. The result is enhanced runner oxidation.

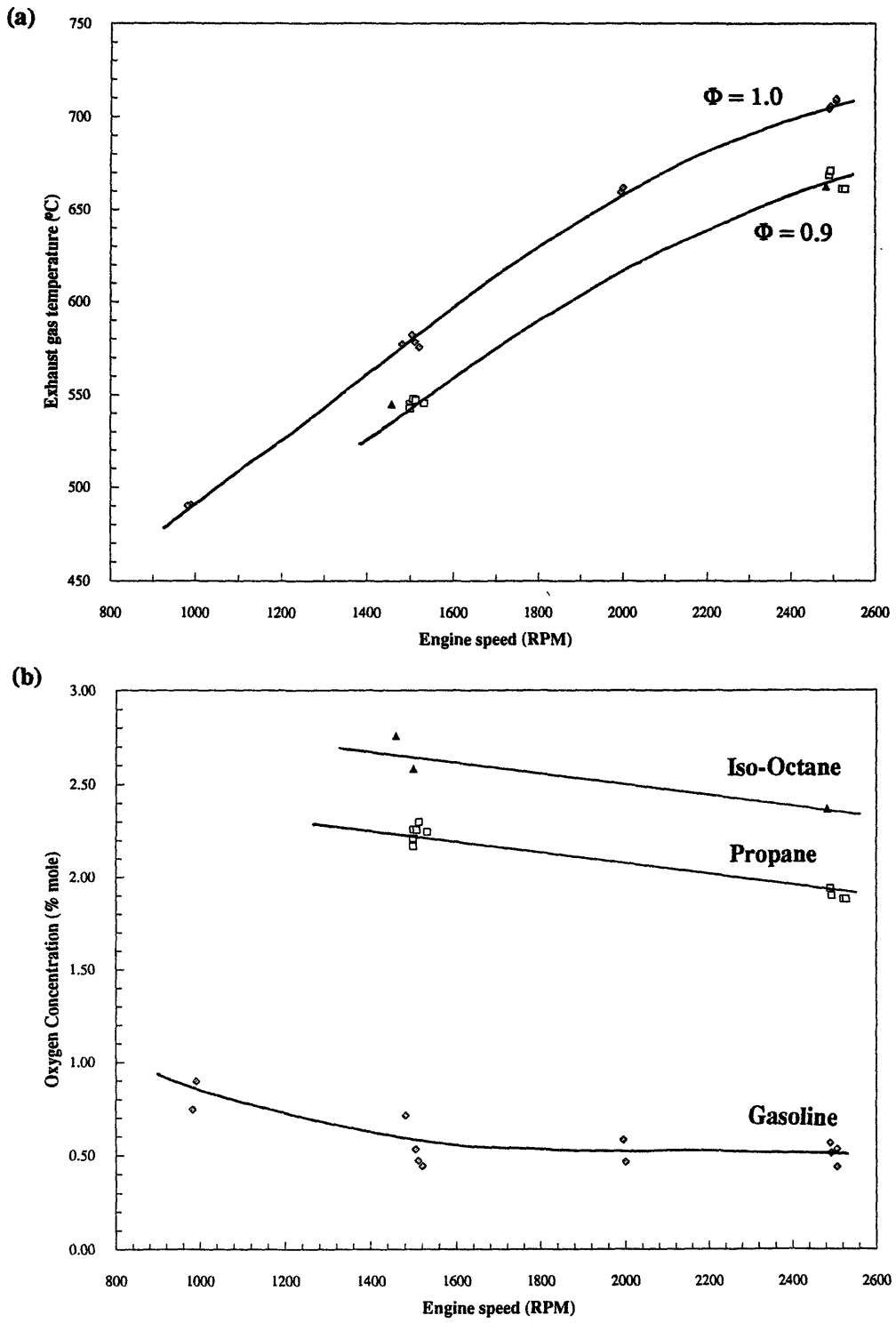

FIGURE 6.1-1 Effect of engine speed on the (a) exhaust gas temperature, (b) exhaust gas O_2 concentration, (c) cylinder-exit HC emissions and (d) overall fraction reduced. Gasoline, iso-octane and propane data were taken at 3.8 bar IMEP, MBT, Φ=0.9 (Φ=1.0 for gasoline) and $T_{coolant}$=88°C.

(c)

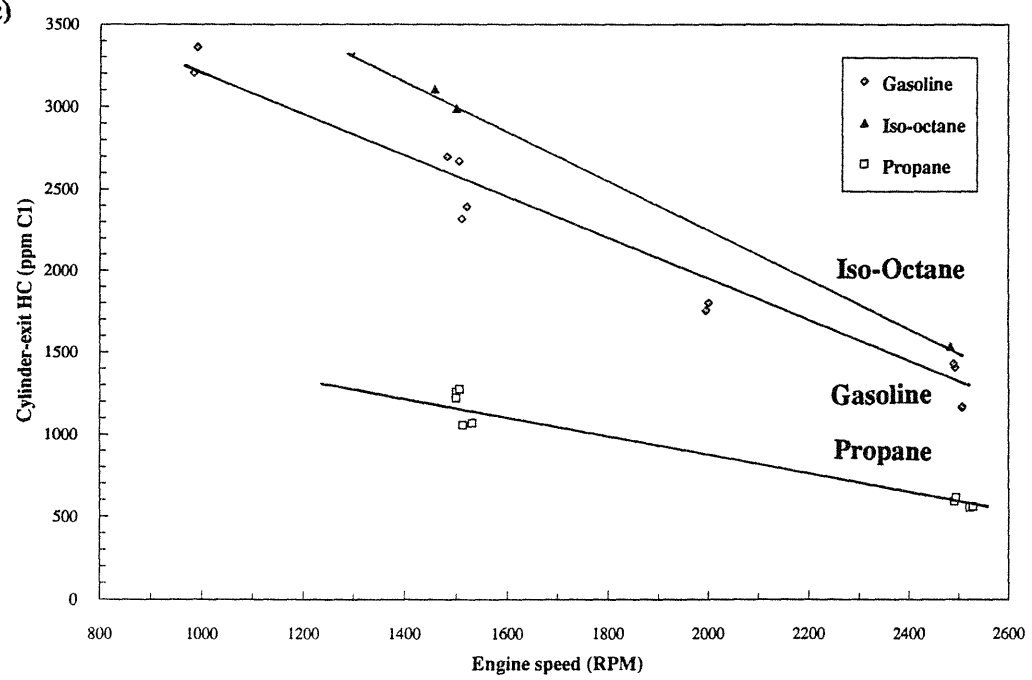

(d)

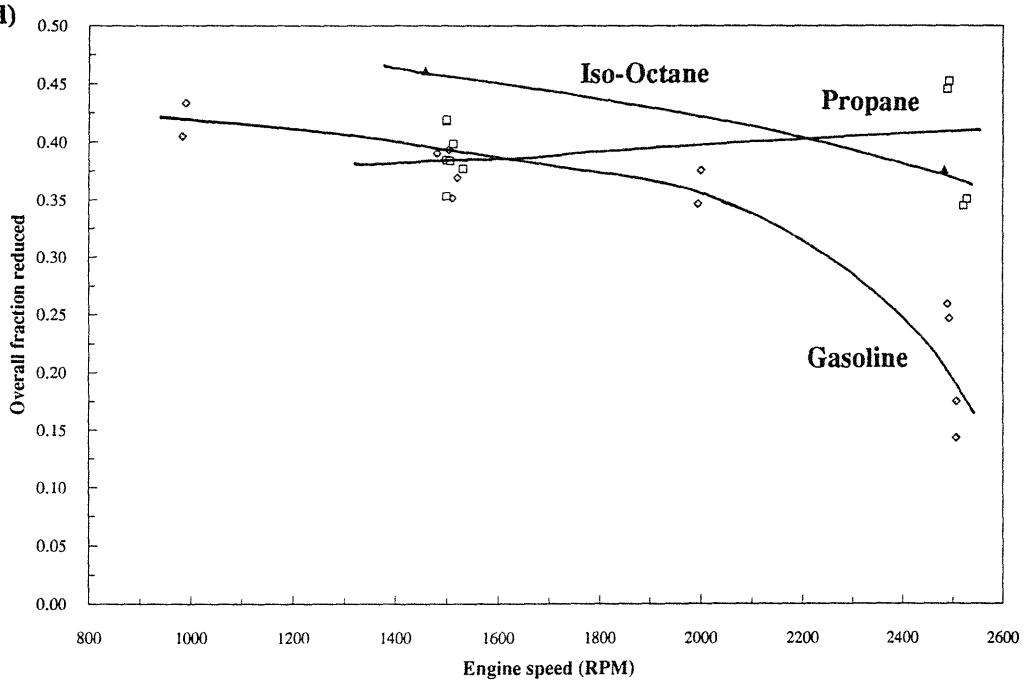

FIGURE 6.1-1 (contd.)

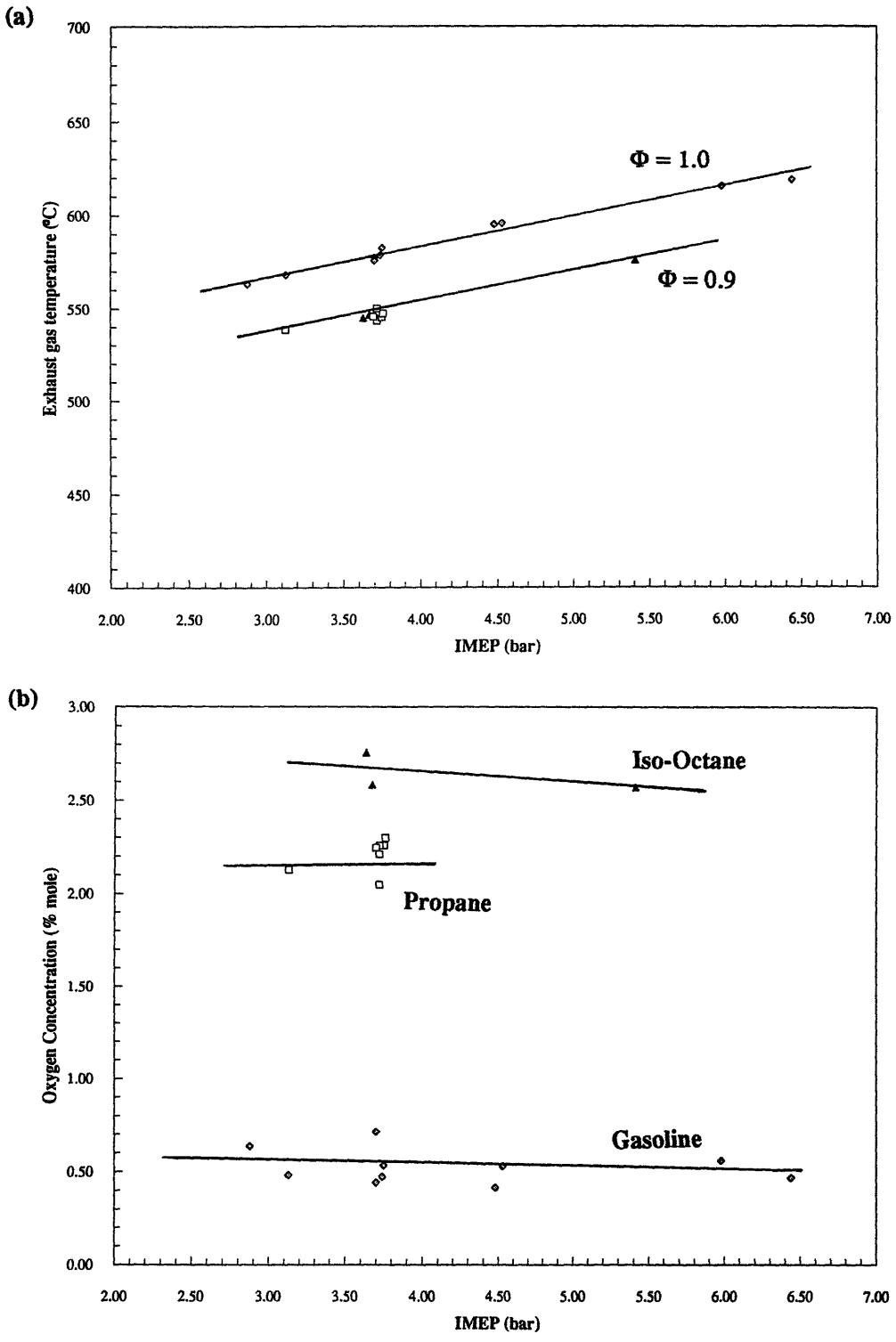

FIGURE 6.2-1 Effect of load on the (a) exhaust gas temperature, (b) exhaust gas O_2 concentration, (c) cylinder-exit HC emissions and (d) overall fraction reduced. Gasoline, iso-octane and propane data were taken at 1500 RPM, MBT, Φ=0.9 (Φ=1.0 for gasoline) and $T_{coolant}$=88°C.

(c)

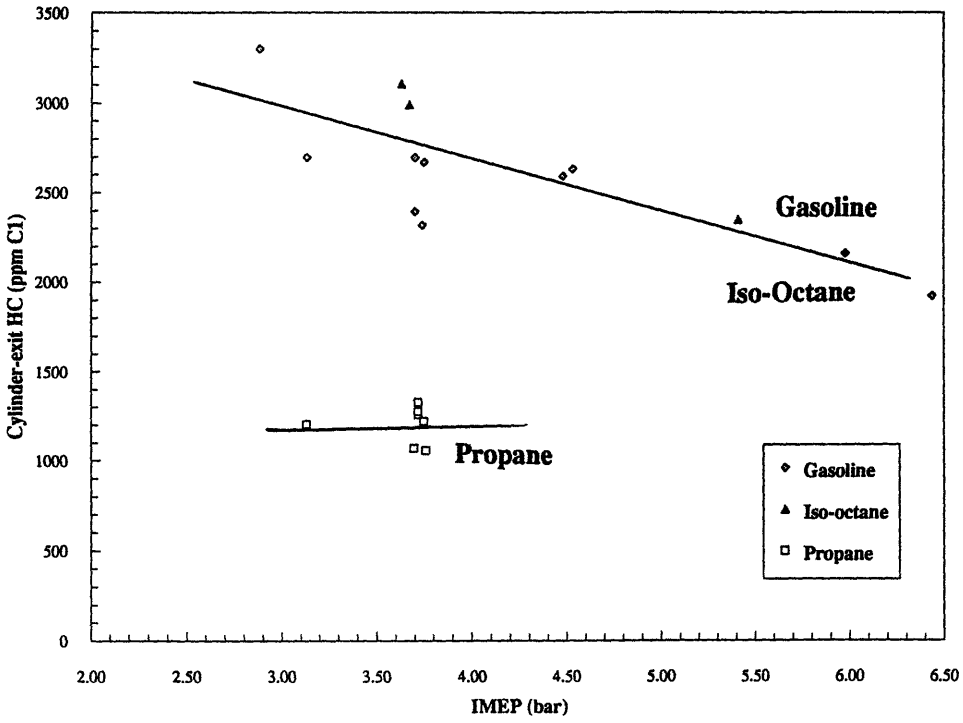

(d)

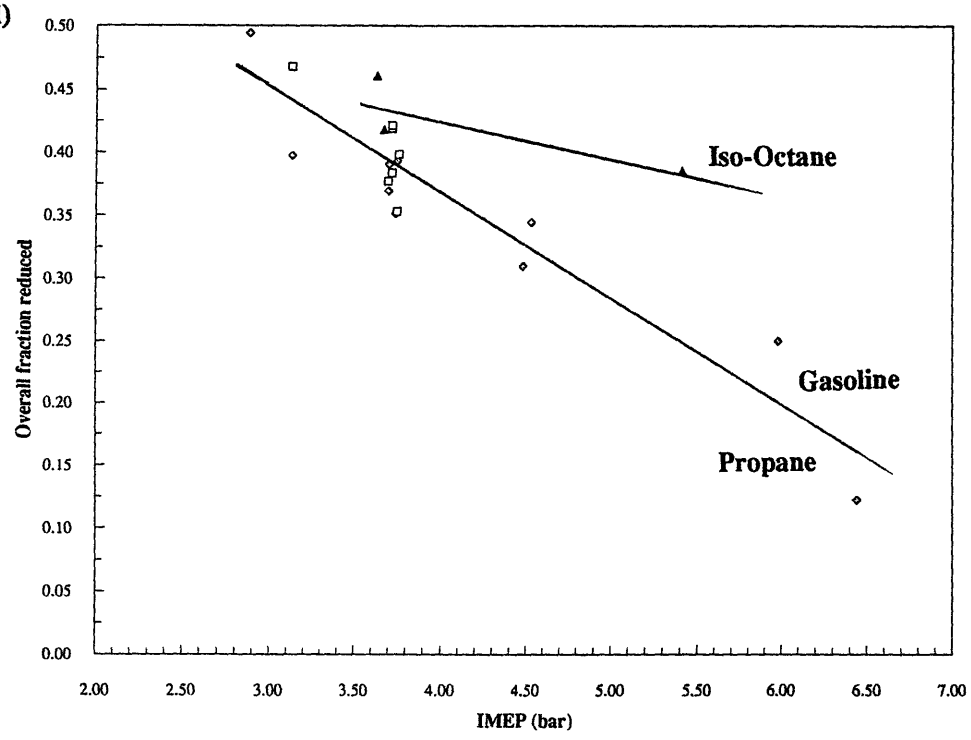

FIGURE 6.2-1 (contd.)

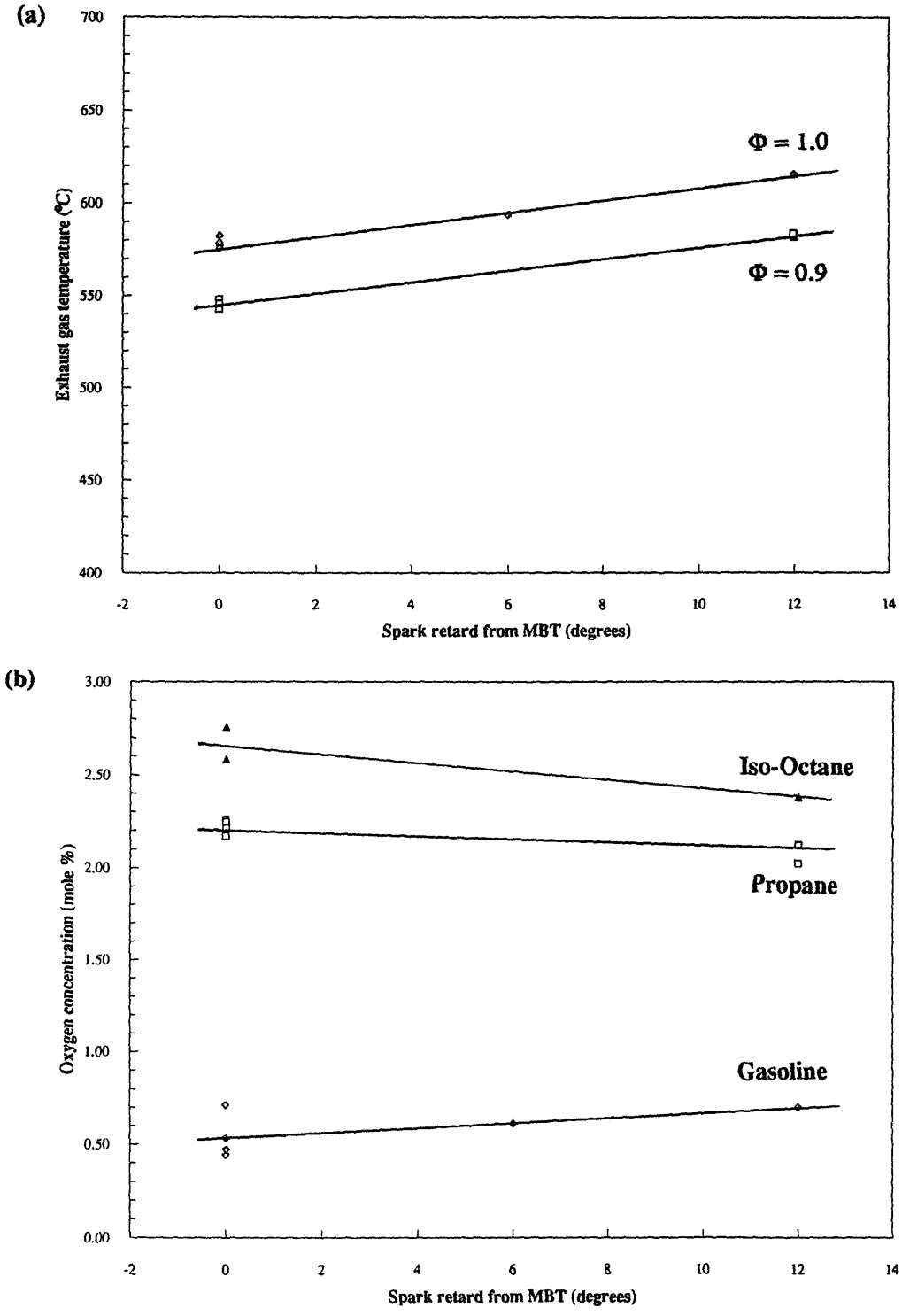

FIGURE 6.3-1 Effect of spark timing on the (a) exhaust gas temperature, (b) exhaust gas O_2 concentration, (c) cylinder-exit HC emissions and (d) overall fraction reduced. Gasoline, iso-octane and propane data were taken at 1500 RPM, 3.8 bar IMEP, Φ=0.9 (Φ=1.0 for gasoline) and $T_{coolant}$=88°C.

(c)

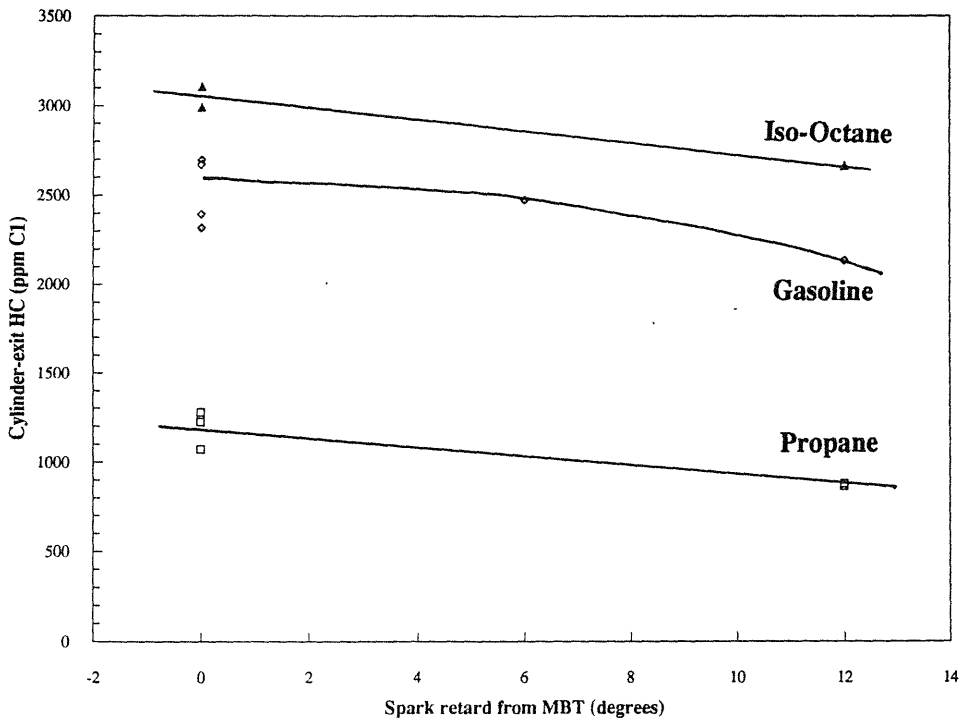

(d)

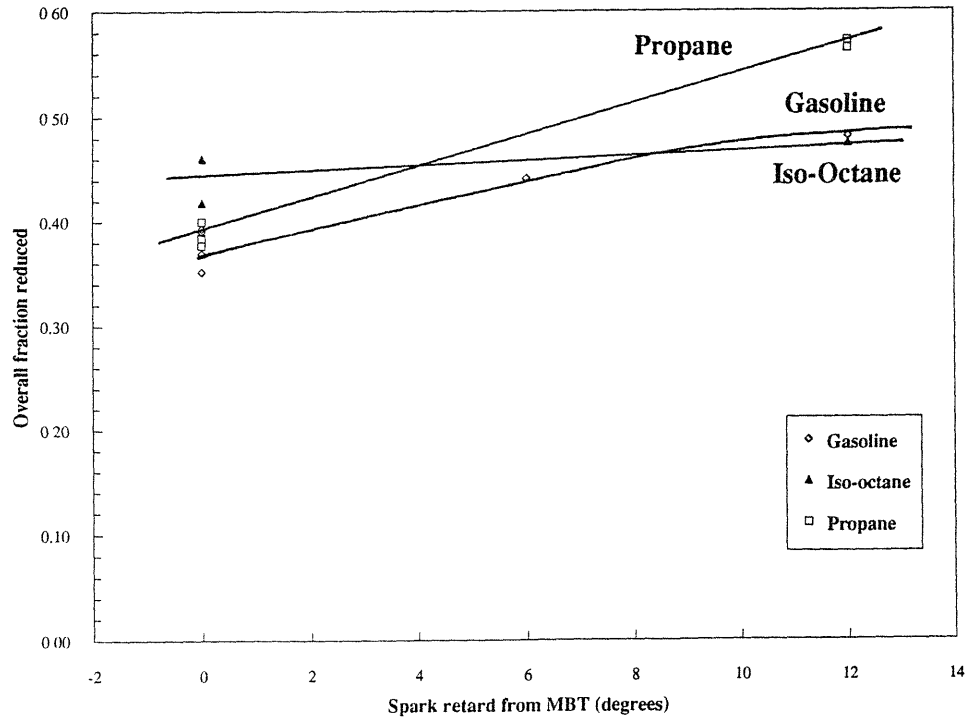

FIGURE 6.3-1 (contd.)

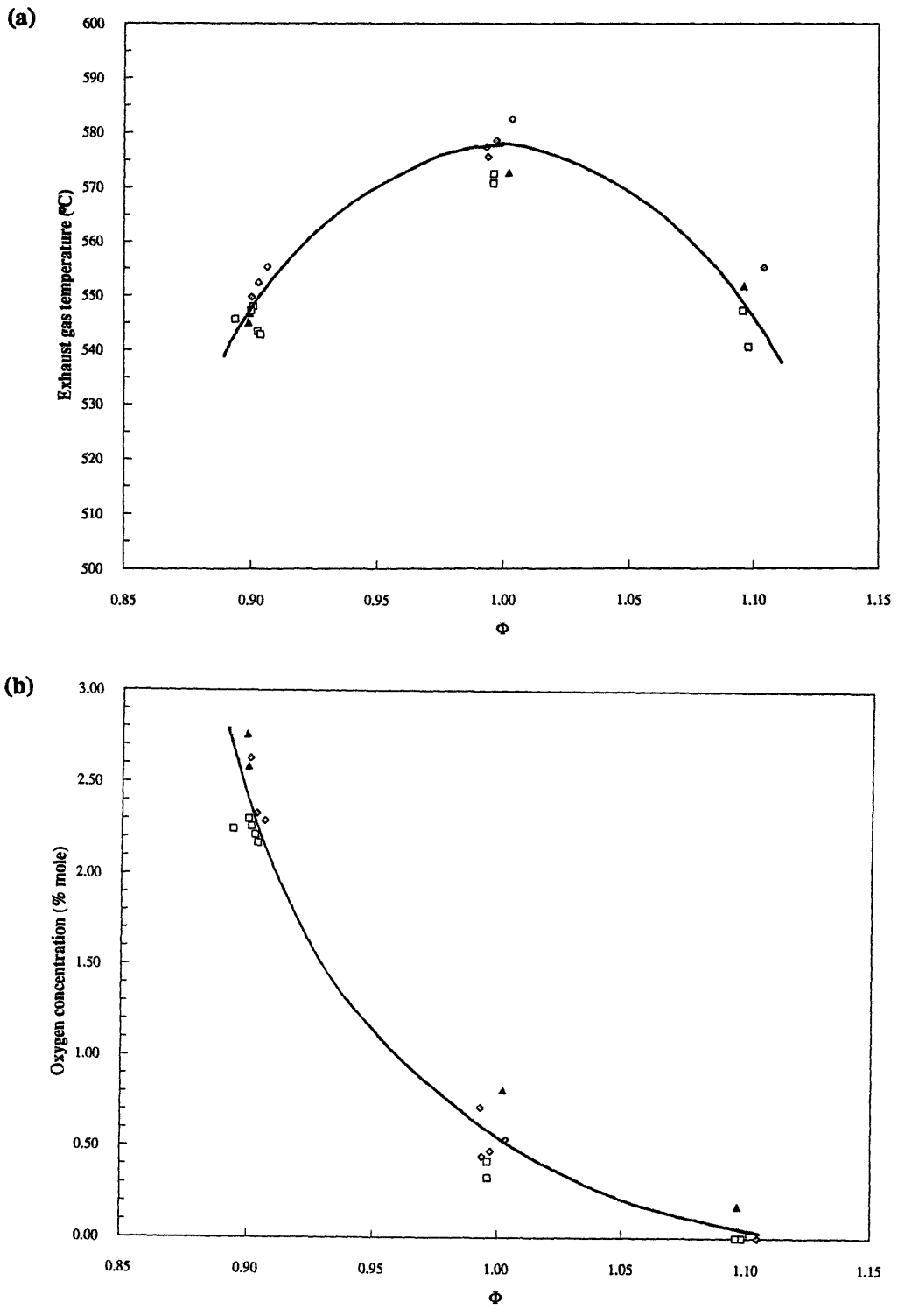

FIGURE 6.4-1 Effect of equivalence ratio (Φ) on the (a) exhaust gas temperature, (b) exhaust gas O_2 concentration, (c) cylinder-exit HC emissions and (d) overall fraction reduced. Gasoline, iso-octane and propane data were taken at 1500 RPM, 3.8 bar IMEP, MBT and $T_{coolant}$=88°C.

(c)

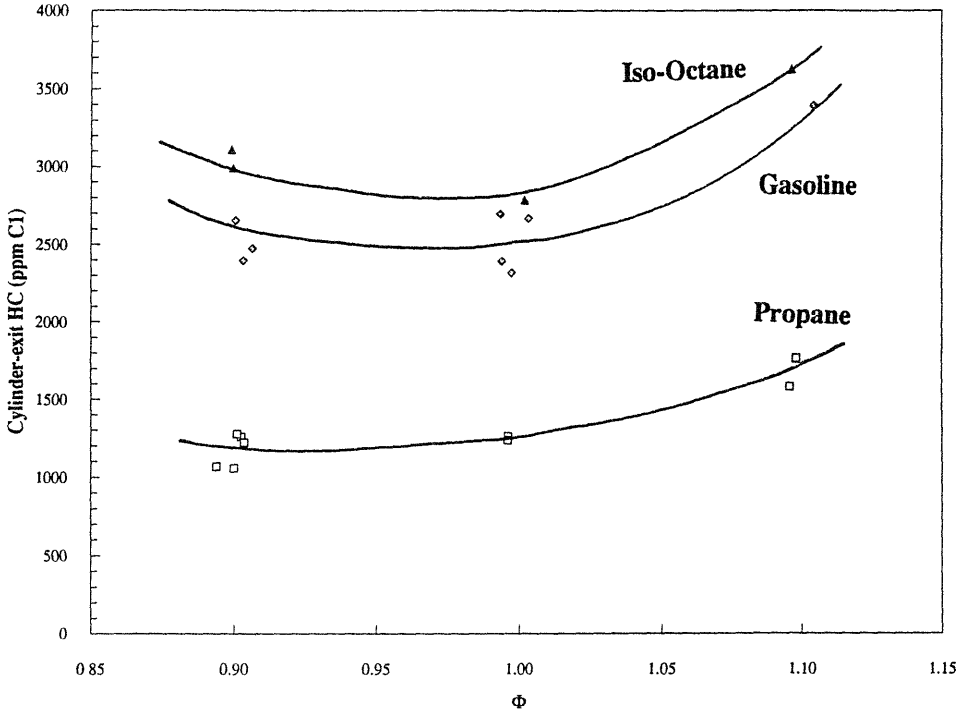

(d)

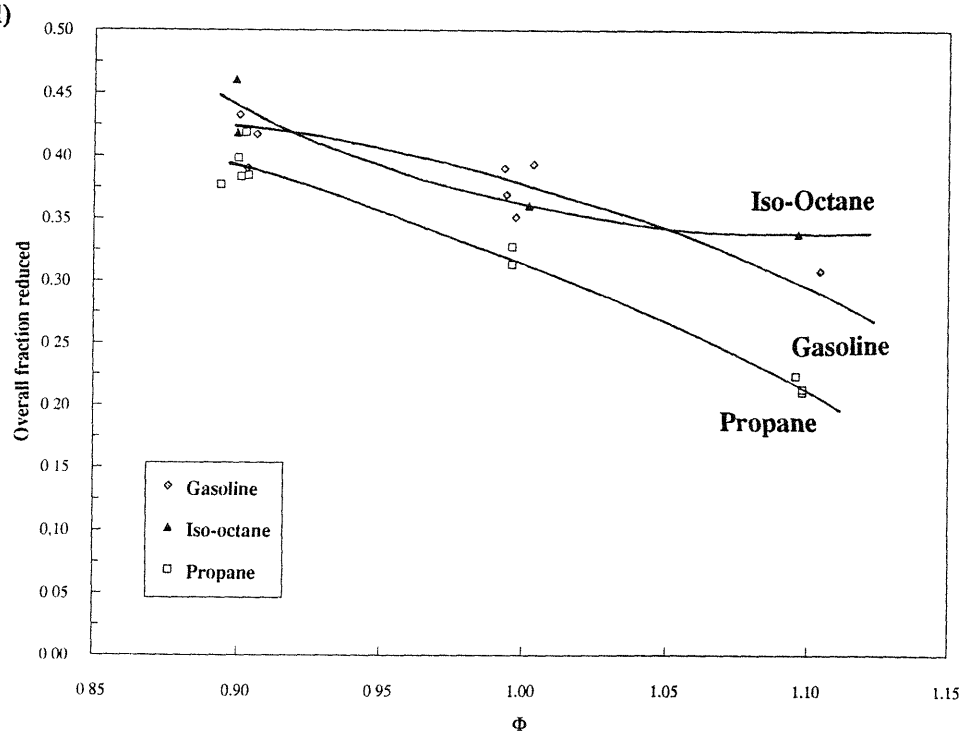

FIGURE 6.4-1 (contd.)

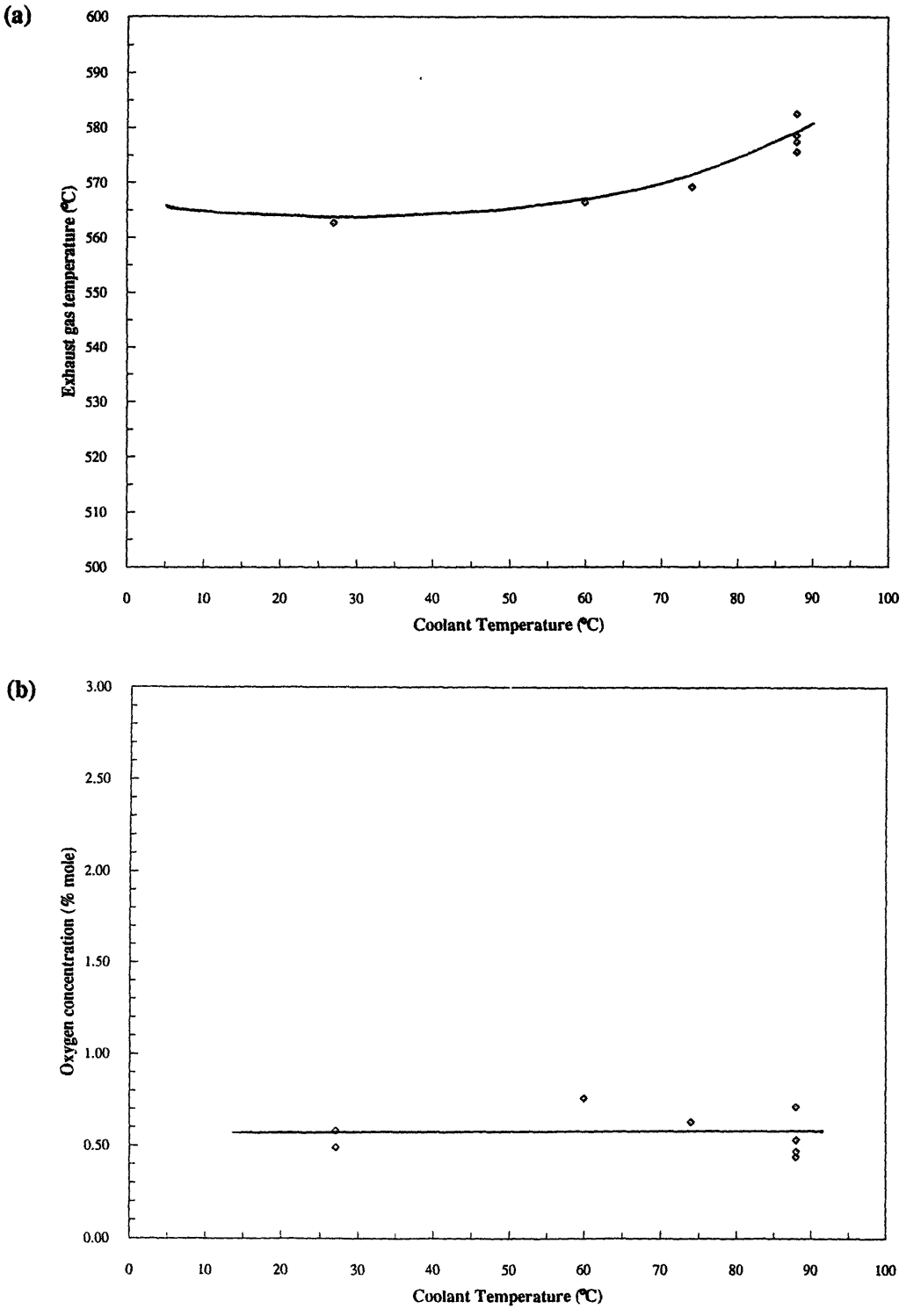

FIGURE 6.5-1 Effect of coolant temperature on the (a) exhaust gas temperature, (b) exhaust gas O_2 concentration, (c) cylinder-exit HC emissions and (d) overall fraction reduced. Gasoline data was taken at 1500 RPM, 3.8 bar IMEP, MBT, and Φ=1.0.

(c)

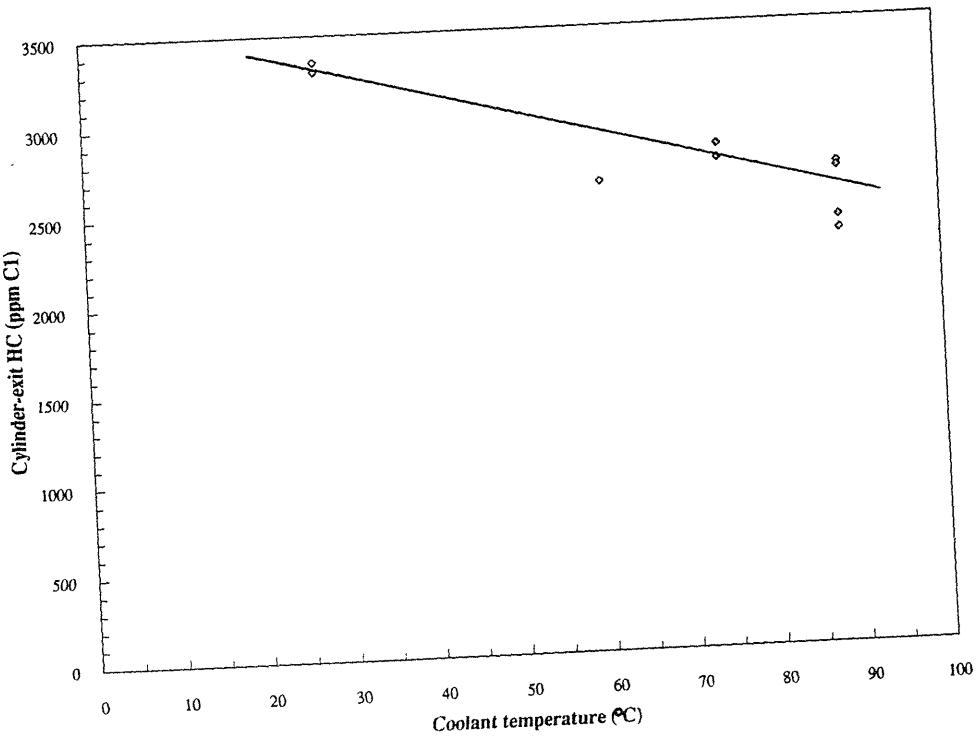

(d)

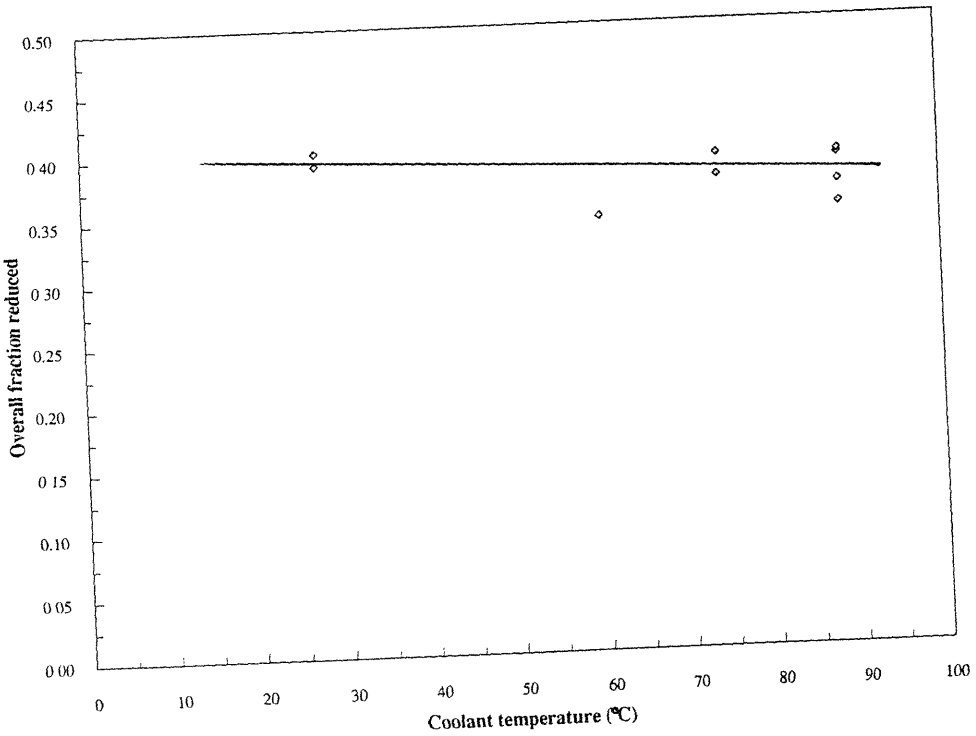

FIGURE 6.5-1 (contd.)

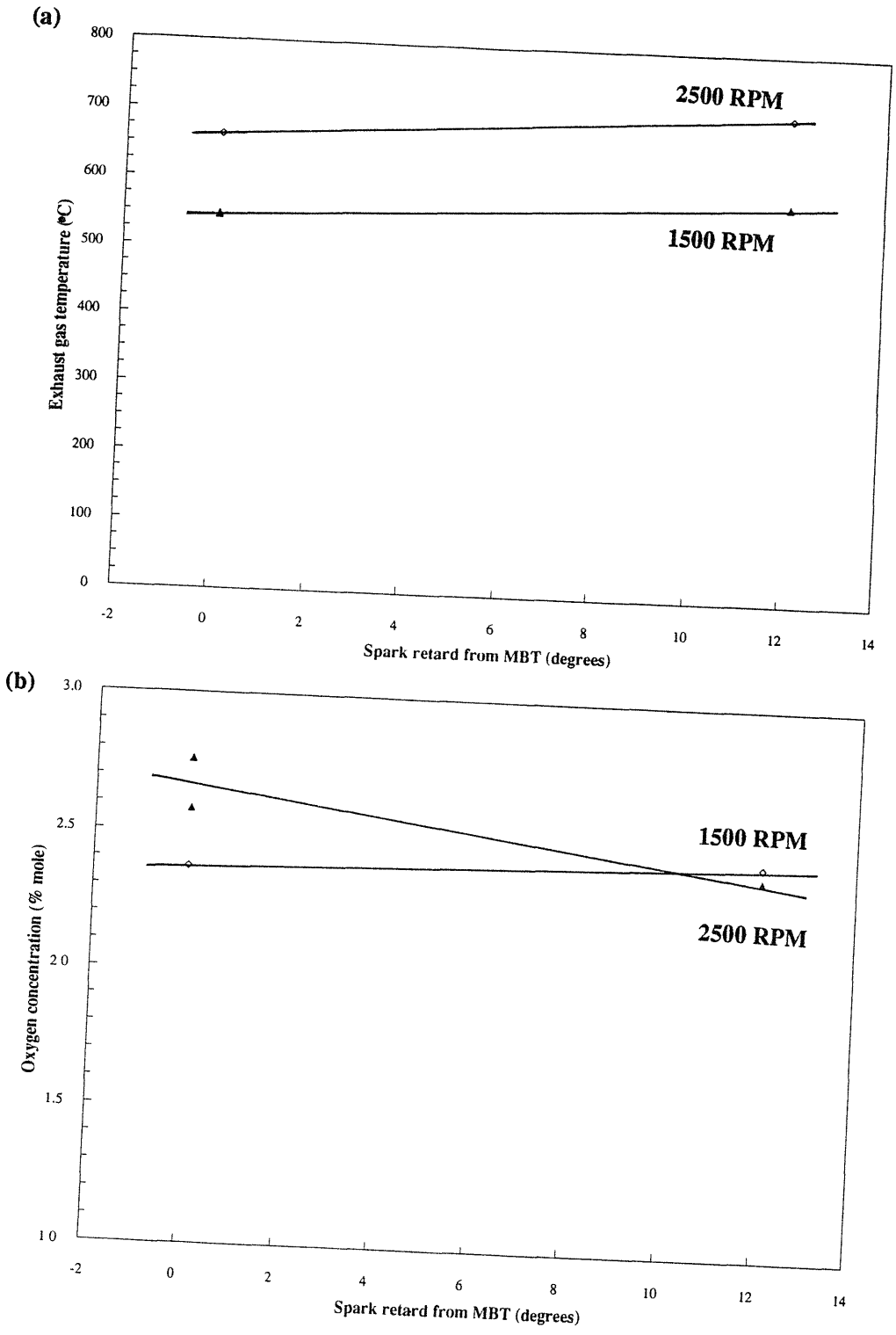

FIGURE 6.6-1 Joint effect of speed and spark timing on the (a) exhaust gas temperature, (b) exhaust gas O_2 concentration, (c) cylinder-exit HC emissions and (d) overall fraction reduced. Iso-octane data was taken at 3.8 bar IMEP (1500 RPM), 4.0 bar IMEP (2500 RPM), Φ=0.9, $T_{coolant}$=88°C.

(c)

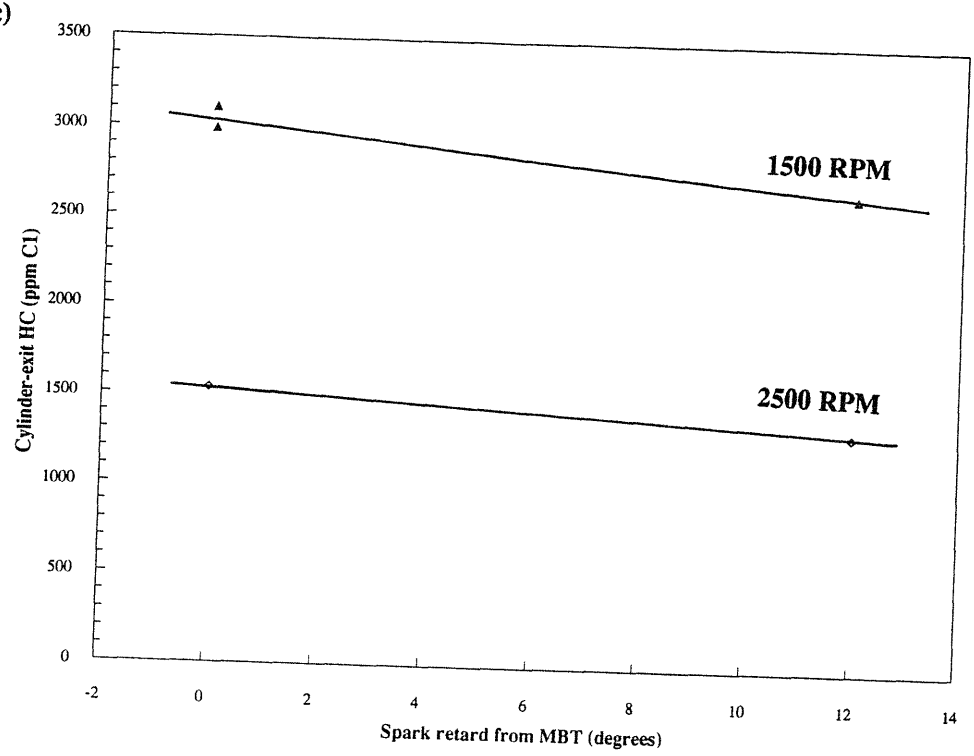

(d)

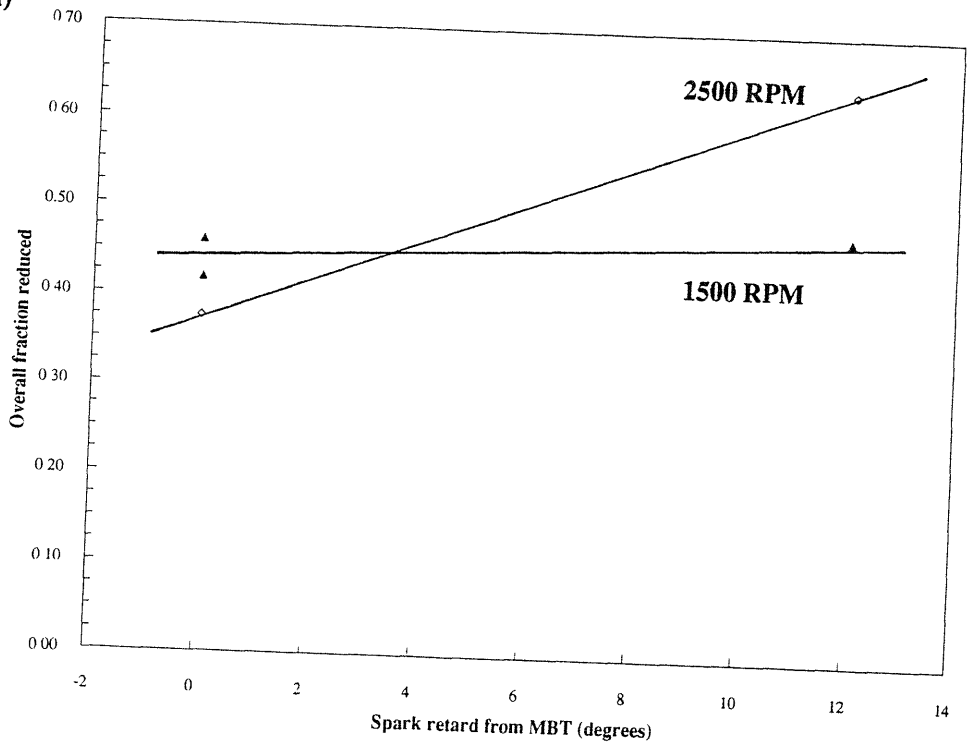

FIGURE 6.6-1 (contd.)

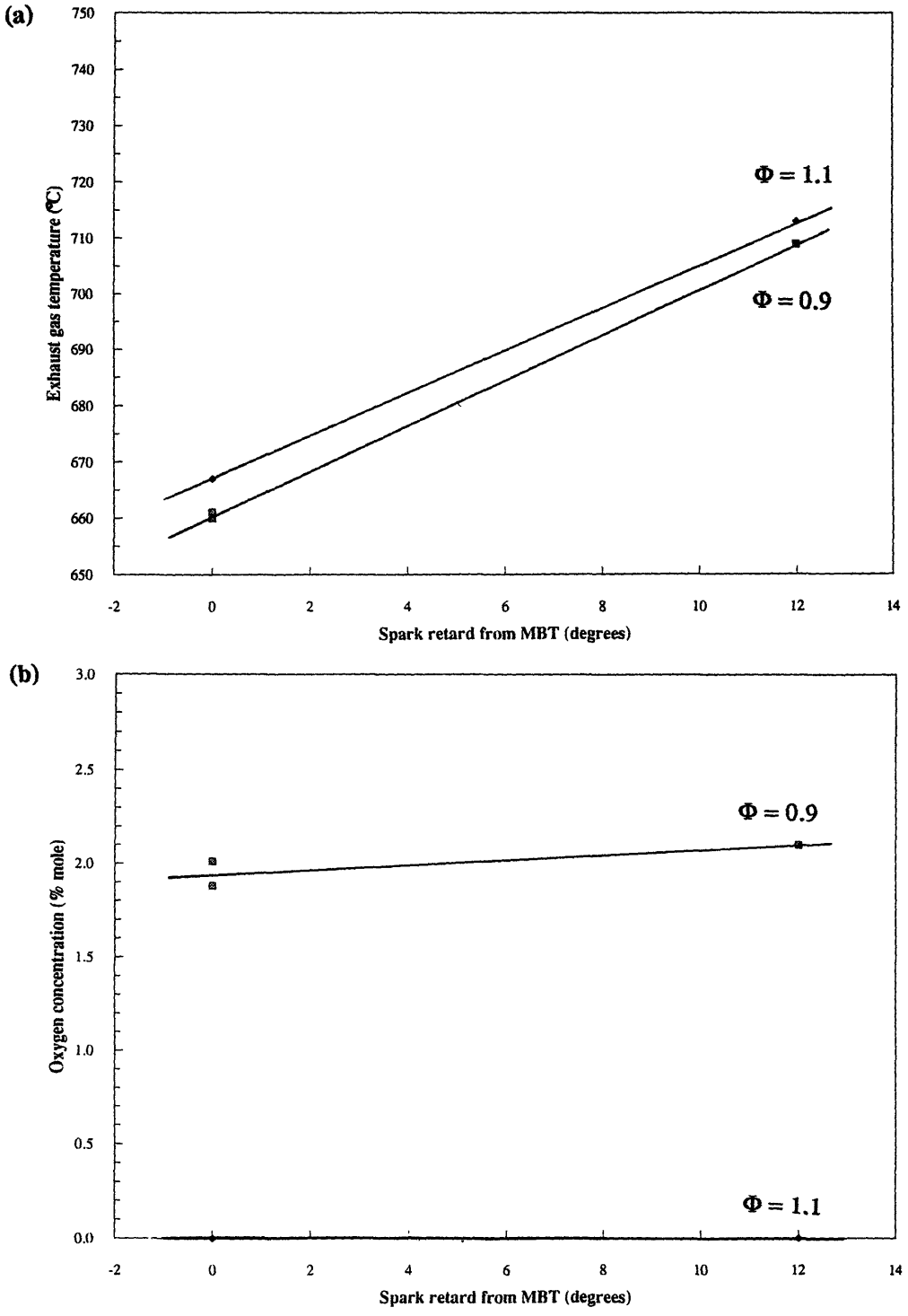

FIGURE 6.6-2 Joint effect of equivalence ratio and spark timing on the (a) exhaust gas temperature, (b) exhaust gas O_2 concentration, (c) cylinder-exit HC emissions and (d) overall fraction reduced. Propane data was taken at 2500 RPM, 4.0 bar IMEP and $T_{coolant}$=88°C.

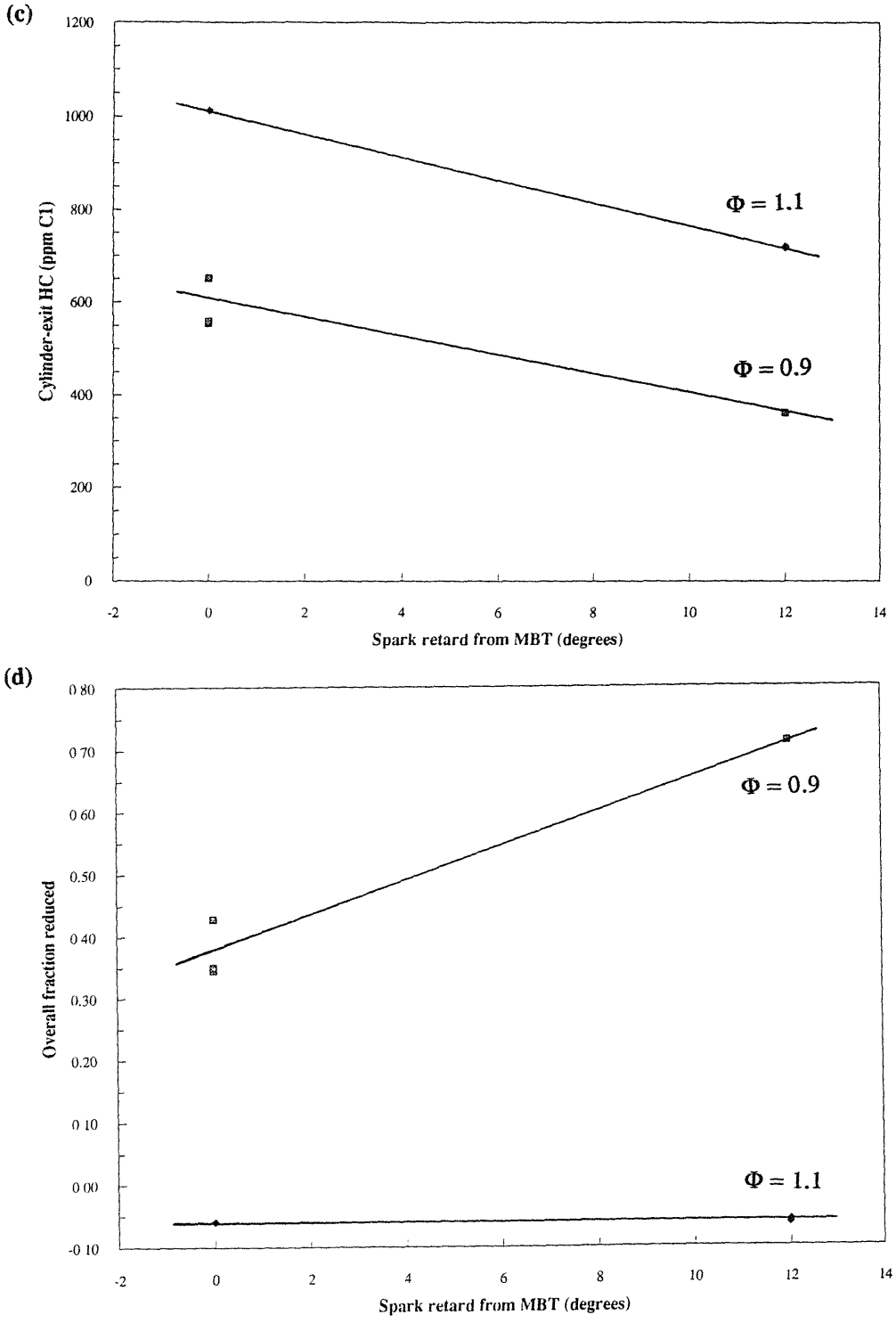

FIGURE 6.6-2 (contd.)

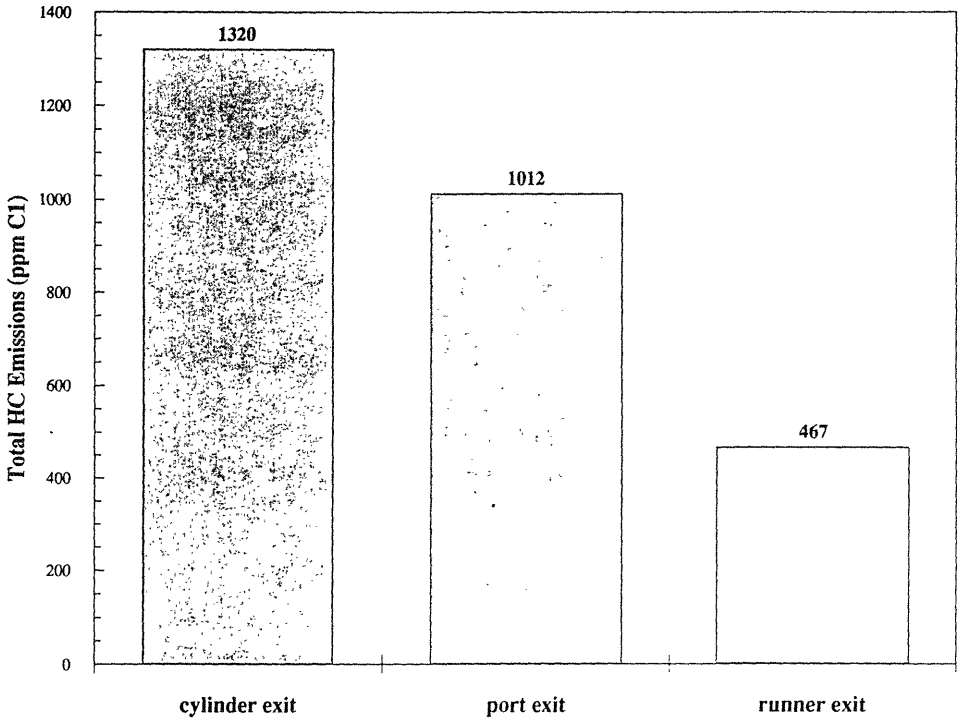

FIGURE 6.6-3 Total HC emissions at the cylinder, port and runner exits for iso-octane. Data was taken at 2500 RPM, 4.0 bar IMEP, 12 degrees retard, Φ=0.9 and $T_{coolant}$=88 °C.

Chapter 7

Conclusions

An exhaust gas quenching experiment was conducted to study the evolution of HC emissions and the extent of HC oxidation in the exhaust port and runner of a spark ignition engine. Fuel composition and engine parameter effects were of particular interest.

The major conclusions drawn from testing a set of fuels at a light load operating were as follows:

1. There was substantial reduction in total HC emissions between the cylinder and the port exit; the reduction is much less in the runner.

2. Differences in cylinder exit HC emissions between the fuels could be explained by differences in HC oxidation rates, oil layer mechanism and molecular diffusivity of the HC.

3. HC oxidation levels in the exhaust port/runner system fell within 40±5% for all the fuels, indicating that HC oxidation was approximately fuel independent at this condition. A majority of the oxidation occurred within the exhaust port.

4. Unburned fuel was the major cylinder exit species. Non-fuel species concentrations did not change significantly from cylinder exit to port exit to reflect the significant level of HC oxidation.

5. Species distributions in both the port and runner changed substantially despite the low levels of runner HC oxidation.

6. HC oxidation of the non-methane alkane fuels was accompanied by an increase in species that are highly reactive in the formation of photochemcial smog.

The major conclusions drawn from several single and multi-parameter sweeps made about a baseline operating condition were as follows:

1. As engine speed increased at constant load, the cylinder-exit HC emissions decreased due to the increase in bulk gas temperature during expansion and a reduced oil layer absorption/desorption mechanism due to a higher liner temperature.

2. HC emissions decreased with increasing load due to a increase in the bulk gas temperature and reduced oil layer contribution.

3. At retarded timing, the increased bulk gas temperature during expansion and exhaust as well as the decreased crevice volume and oil film contributions governed the cylinder-exit HC emissions and the HC oxidation.

4. Despite the increase in exhaust gas temperature, HC oxidation decreased going from lean to stoichiometric due to a lack of available O_2. Oxidation levels continued to drop as the charge was enriched due to both the lack of O_2 and the decrease in exhaust temperature.

5. As coolant temperature increased, the cylinder exit HC emissions were reduced. HC oxidation did not change indicating that a significant fraction of oxidation may occur in-cylinder.

6. The combination of high speed, retarded spark timing and lean operating condition yielded high levels of HC oxidation.

References

[1] The Federal Clean Air Act, Title II, Public Law 101-549, amended November 1990; the Low Emissions Vehicle/Clean Fuels Program, approved by the California Air Resources Board, September 1990.

[2] Lowi, A. and Carter, W.P.L., "A Method for Evaluating the Atmospheric Ozone Impact of Actual Vehicle Emissions," SAE paper 900710, 1990.

[3] Cheng, W.K., Hamrin, D., Heywood, J.B., Hochgreb, S., Min, K., and Norris, M., "An Overview of Hydrocarbon Emissions Mechanisms in Spark-Ignition Engines," SAE paper 932708, 1993.

[4] Kaiser, E.W., Siegl, W.O., Henig, Y.I., Anderson, R.W. and Trinker, F.H., "Effect of Fuel Structure on Emissions from a Spark-Ignited Engine," *Environmental Science and Technology*, 1991, Vol. 25, No. 12, pp. 2005-2012.

[5] Min, K, "The Effects of Crevices on the Engine-out Hydrocarbon Emissions in Spark Ignition Engines," Ph.D. Thesis, Department of Mechanical Engineering, M.I.T., February, 1994.

[6] Mendillo, J.V. and Heywood, J.B., "Hydrocarbon Oxidation in the Exhaust Port of a Spark Ignition Engine," SAE paper 810019, 1981.

[7] Caton, J.A. and Heywood, J.B., "Models for Heat Transfer, Mixing and Hydrocarbon Oxidation in an Exhaust Port of a Spark-Ignited Engine," SAE paper 800290, 1980.

[8] Wu, K., "Chemical Kinetic Modeling of Oxidation of Hydrocarbon Emissions in Spark Ignition Engines," Master's Thesis, Department of Mechanical Engineering, M.I.T., February, 1994.

[9] Adamcyzk, A.A. and Kach, R.A., *Combustion Science Technology*, 1986, 47, 193.

[10] Schramm, J. and Sorenson, S.C., "Solubility of gasoline components in different lubricants for combustion engines determined by gas-liquid partition chromatography," *Journal of Chromatography*, 1991, 538, pp. 241-248.

[11] Gatellier, B., Trapy, J., Herrier, D., Quelin, J.M., Galliot, F., "Hydrocarbon Emissions of SI Engines as Influenced by Fuel Absorption-Desorption in Oil Films," SAE paper 920095, 1992.

[12] Tsuchida, H., Ishihara, K., Iwakiri, Y. and Matsumoto, M., "Effect of Catalyst Systems on Characteristics of Exhaust Hydrocarbon Species," SAE paper 932718, 1993.

[13] Schramm, J. and Sorenson, S.C., "A Model for Hydrocarbon Emissions from SI Engines," SAE paper 902169, 1990.

[14] Heywood, J.B., Internal Combustion Engine Fundamentals, McGraw-Hill, Inc., New York, 1988.

Appendix A

Index of Total and Speciated HC Emissions Data Available for a Given Variation in Engine Parameter or Fuel Composition

FUEL	Fuel Composition Effects			Engine Operating Parameters				
	Cylinder Exit	Port Exit	Speciated Emissions	Speed	IMEP	Spark	Coolant	Φ
Gasoline	yes	yes	yes	yes	yes	yes	yes	yes
Methane	yes	yes	yes	no	no	no	no	partial
Ethane	yes	no	yes	no	no	no	no	no
Propane	yes	yes	yes	yes	partial	partial	no	yes
n-Butane	yes	no	yes	no	no	no	no	no
Iso-octane	yes	yes	yes	partial	partial	partial	no	yes
Ethene	yes	no	yes	no	no	partial	no	partial
Toluene	yes	yes	yes	no	no	no	no	no

* Some joint variations were also carried out.

Appendix B

Formulation of the HC Emissions Correction Factor

As described in Section 3.3, emissions measurements were made under a number of different exhaust conditions and were as follows: (1) normal, (2) quench gas injected, (3) quench gas injected and air diluted, and (4) air diluted. Definitions for all exhaust mole species eeither coming from the engine or added to the exhaust are indicated in Figure B.1-1. The significant measurements made under these ehxaust conditions were:

$$(1) \qquad (x_{CO_2})_{Exhaust,dry} \equiv \alpha \qquad \text{(B.1)}$$

$$(x_{HC})_{Exhaust,wet} \qquad \text{(B.2)}$$

$$(2) \qquad (x_{HC})_{Quench,wet} \qquad \text{(B.3)}$$

$$(3) \qquad (x_{CO_2})_{(Dilution+Quench),dry} \equiv \beta \qquad \text{(B.4)}$$

$$(4) \qquad (x_{CO_2})_{Dilution,dry} \equiv \gamma \qquad \text{(B.5)}$$

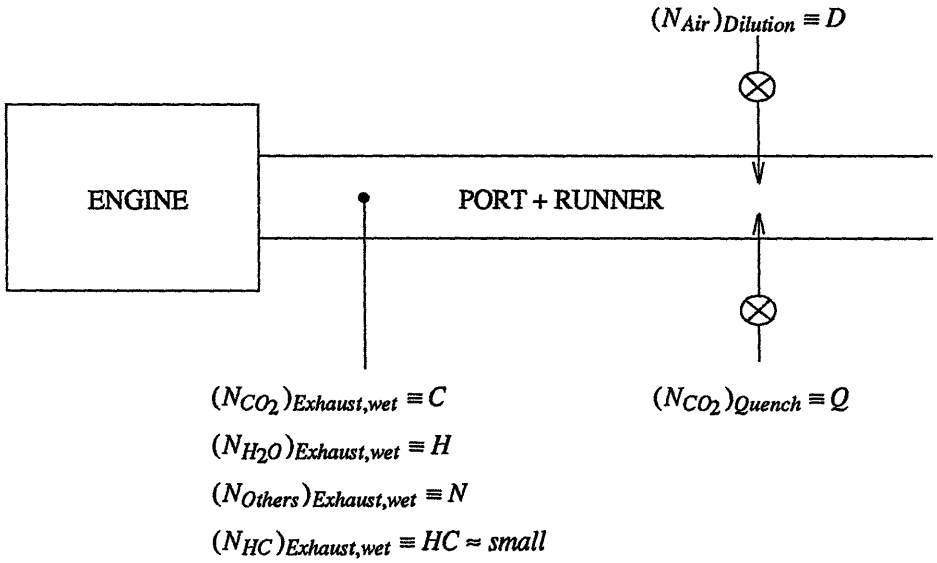

FIGURE B.1-1 Definitions for the species exiting the engine and the species added to the exhaust.

With the exception of the HC measurements (B.2 and B.3), all measurements were dry. For consistency, water's contribution was added. It was defined as

$$(x_{H_2O})_{Exhaust} \equiv \xi \tag{B.6}$$

and calculated using [14]

$$(H_2O) = 0.5y\frac{(CO_2)+(CO)}{(CO)/[K(CO_2)]+1}$$

where y is the H/C ratio of the fuel, K equals 3.5 and the CO and CO_2 mole fractions were measured under normal exhaust conditions. When equations B.1, 4, 5 and 6 were rewritten using the definitions in Figure B.1-1 and then normalized by C (where the lower case symbols represent the normalized values), they became

$$(x_{CO_2})_{Exhaust,dry} = \frac{C}{C+N} = \frac{1}{1+n} \equiv \alpha \tag{B.7}$$

$$(x_{CO_2})_{(Dilution+Quench),dry} = \frac{C+Q}{C+N+Q+D} = \frac{1+q}{1+n+q+d} \equiv \beta \tag{B.8}$$

$$(x_{CO_2})_{Dilution,dry} = \frac{C}{C+N+D} = \frac{1}{1+n+d} \equiv \gamma \tag{B.9}$$

$$(x_{H_2O})_{Exhaust} = \frac{H}{C+N+H} = \frac{h}{1+n+h} \equiv \xi \tag{B.10}$$

where the HC contribution was neglected because its contribution was small compared to the others. This system of four equations with known values α, β, γ and ξ was solved for the unknowns yielding

$$n = \frac{1}{\alpha} - 1 \tag{B.11}$$

$$q = \frac{\beta - \gamma}{\gamma(1-\beta)} \tag{B.12}$$

$$d = \frac{1}{\gamma} - \frac{1}{\alpha} \tag{B.13}$$

$$h = \frac{\xi}{\alpha(1-\xi)} \tag{B.14}$$

Recall that the goal in developing an emissions correction factor was to translate $(x_{HC})_{Quench,wet}$ (B.3) to $(x_{HC})_{Corrected,wet}$,the equivalent HC concentration under normal exhaust conditions. Ratioing the two and rewriting it in terms of the definitions in Figure B.1-1 resulted in

$$\frac{(x_{HC})_{Quench,wet}}{(x_{HC})_{Exhaust,wet}} = \frac{HC/(C+N+H+Q)}{HC/(C+N+H)}$$

Simplifying and normalizing by C gave

$$\frac{(x_{HC})_{Quench,wet}}{(x_{HC})_{Exhaust,wet}} = \frac{(1+n+h)}{(1+n+h+q)} \qquad \text{(B.15)}$$

with n, q and h defined as before. Substituting equations B.11, 12 and 14 into B.15, the equation became

$$\frac{(x_{HC})_{Quench,wet}}{(x_{HC})_{Corrected,wet}} = \frac{1-(x_{CO_2})_{Quench,wet}}{1-(x_{CO_2})_{Exhaust,wet}} \qquad \text{(B.16)}$$

where $(x_{HC})_{Corrected,wet}$ was the variable to be solved. Although equation B.16 was developed for the HC emissions, it was a general equation that could be used to correct any exhaust species that was diluted due quench gas injection.